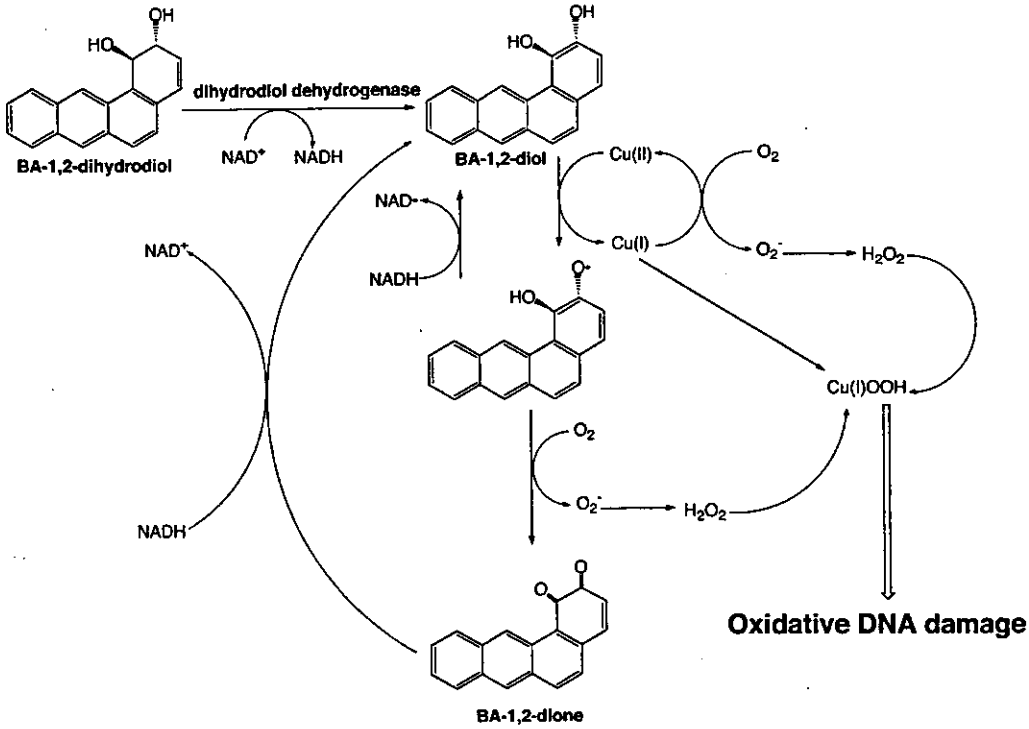

Figure 7. Proposed mechanism of Cu(II)-mediated oxidative DNA damage induced by BA-1,2-dihydrodiol metabolite.

$-\Delta H$ for dehydrogenation to catechol. The correlation coefficiency between NADH production and $-\Delta H$ was 0.8063 ($P = 0.0992$). These results have shown that BA–1,2-dihydrodiol can be most easily converted into the corresponding catechol form, BA-1,2-diol.

Detection of the Product in the Reaction of BA–1,2-Dihydrodiol, DD, and NAD$^+$. Figure 6 shows mass spectra of the reaction product of BA–1,2-dihydrodiol before and after enzymatic reaction. Figure 6A shows the mass spectrum with a molecular ion at *m/z* 262 (M^+) assigned to BA–1,2-dihydrodiol before the reaction. The peak with a molecular ion at *m/z* 260 (M^+) appeared after the reaction (Figure 6B, arrow). This peak is attributed to the catechol type metabolite, BA–1,2-diol, generated by the treatment of DD.

Calculated HOMO Energy of BA–Diols and B[*a*]P–7,8-Diol. Calculated HOMO energies of BA–diols and B[*a*]P–7,8-diol were as follows: 6.94 (BA–1,2-diol), 7.05 (BA–5,6-diol), 7.13 (BA–8,9-diol), 6.91 (BA–10,11-diol), and 6.69 (B[*a*]P–7,8-diol) eV. These calculated values suggest that the tendencies of autoxidation of these BA–diols and B[*a*]P–7,8-diol are in the following order: B[*a*]P–7,8-diol > BA–10,11-diol > BA–1,2-diol > BA–5,6-diol > BA–8,9-diol. The DNA damaging activity of B[*a*]P–7,8-diol may be explained by the tendency of autoxidation of the corresponding catechol forms in addition to the above-mentioned $-\Delta H$.

Discussion

We revealed that BA–1,2-dihydrodiol and B[*a*]P–7,8-dihydrodiol induced Cu(II)-mediated oxidative DNA damage in the presence of DD, but other BA–dihydrodiols did not under the condition used. The observation of NADH production suggested that DD catalyzed BA–1,2-dihydrodiol most efficiently to its catechol among PAH–dihydrodiols tested. We also showed that BA–1,2-dihydrodiol induced Cu(II)-mediated 8-oxodG formation with DD treatment. BA–1,2-dihydrodiol significantly induced a G lesion at the 5′-ACG-3′ sequence complementary to codon 273 of the *p53* tumor suppressor gene. This sequence is known as a hotspot where mutations occurred in high frequency (*15*). An analysis of the *p53* mutational database shows that G to T transversion is a signature mutation of lung cancer. Because 8-oxodG formation can lead to G to T transvertion, 8-oxodG has attracted much attention in relation to PAH-induced lung carcinogenesis. These results suggested that DD converted BA–1,2-dihydrodiol to BA–1,2-diol, which induced metal-dependent oxidative DNA damage including 8-oxodG formation via the quinone–catechol redox cycle. Our previous study (*16*) and Flowers et al. (*17*) showed that B[*a*]P–7,8-dione induced oxidative DNA damage via the quinone–catechol redox cycle. Penning and his colleagues (*18*) examined reactive oxygen species (ROS) generation and mutations in yeast by B[*a*]P–7,8-dione. These observations on B[*a*]P–dione may be explained by assuming that AKRs activate PAH *trans*-dihydrodiols to yield *o*-quinone (*19*). It is noteworthy to demonstrate that PAH–dihydrodiols can induce oxidative DNA damage in the presence of DD.

Catalase and bathocuproine inhibited Cu(II)-mediated DNA damage by BA–1,2-dihydrodiol metabolite, indicating the involvement of H_2O_2 and Cu(I). These reactive species were certainly generated during the quinone–catechol redox cycle process of BA–1,2-dihydrodiol metabolite. On the basis of these results and references, a possible mechanism of oxidative DNA damage by BA–1,2-dihydrodiol can be explained as follows (Figure 7); DD catalyzes NAD$^+$-linked oxidation of BA–1,2-dihydrodiol to BA–1,2-diol, the catechol form. It is autooxidized into the corresponding semiquinone radical with concomitant generation of Cu(I) and $O_2^{\cdot-}$. $O_2^{\cdot-}$ dismutates to H_2O_2, which interacts with Cu(I) to form a copper–hydroperoxo complex such as Cu(I)OOH. Furthermore, NADH nonenzymatically reduces BA–1,2-dione into BA–1,2-diol through two-electron reduction-forming re-

dox cycles, such as benzene–catechol (*20*). Therefore, PAH–dihydrodiols and DD may play an important role in oxidative DNA damage via BA *o*-quinones/catechols redox cycling.

Palakal et al. reported that DD preferentially oxidized B[*a*]P–7,8-dihydrodiol and BA–3,4-dihydrodiol (*18*). We showed that BA–1,2-dihydrodiol was more efficiently oxidized to catechol form by DD than B[*a*]P–7,8-dihydrodiol and other BA–dihydrodiols. Reasonably, BA–1,2-dihydrodiol can cause most efficiently oxidative DNA damage with enzymatic metabolic activation by DD, although it is a minor metabolite. Multiple human tissue expression array analyses showed expression of DD, suggesting that this pathway of PAH activation may be widespread in human tissue (*18*). DD has dual toxicological roles in the metabolism of PAHs (*19*, *21*). The enzyme suppresses the formation of their carcinogenic dihydrodiol epoxides and DNA adducts, whereas it yields catechol and quinones, resulting in oxidative DNA damage. Reports concerning overexpression of DD in lung cancer and hepatocellular carcinoma (*8*, *9*) may suggest the involvement of oxidative DNA damage in a carcinogenic process. Therefore, it is important to clarify the theoretically reactive mechanism for the dehydrogenation of substrate by DD and autoxidation of the corresponding catechols. The most efficient dehydrogenation in BA–1,2-dihydrodiol can be explained by the highest $-\Delta H$ of the reaction. The production of catechol and NADH increased almost depending on the $-\Delta H$ of dehydrogenation. The degrees of dehydrogenation are involved in $-\Delta H$ of substrates and partly affinity between enzyme and dihydrodiols. On the other hand, ROS generation activity of catechols (BA–diols and B[*a*]P–diol) depends on the oxidation potential, which is almost consistent with the HOMO energy. Among compounds used in this study, the highest DNA-damaging activity of BA–1,2-dihydrodiol can be reasonably explained by the highest $-\Delta H$, which means tendency of conversion to the catechol form. In addition, the highest HOMO energy of B[*a*]P–7,8-diol among the corresponding diols may contribute to relatively strong DNA-damaging activity, although its $-\Delta H$ is not so high. Collectively, it is suggested that the oxidative DNA-damaging activity of BA–dihydrodiols and B[*a*]P–dihydrodiol may depend on $-\Delta H$ of dehydrogenation and the HOMO energy.

Chen et al. demonstrated that DD overexpression was assosiated with lung cancer (*8*). DD catalyzes PAH–dihydrodiols to catechols, resulting in quinone toxicity including alkylation and oxidative stress (*21*). DD may play an important role in BA carcinogenesis. It is interesting to find that DD-catalyzed BA–1,2-dihydrodiol can induce oxidative DNA damage involving G damage of ACG sequence complementary to codon 273 of the *p53* tumor suppressor gene, a mutational hotspot in lung cancer. Recently, we showed that BA–3,4-dihydrodiol nonenzymatically induced oxidative DNA damage via a unique nonquinone redox cycle (*22*). Our present and previous studies have shown a possibility that oxidative DNA damage by BA metabolites, especially BA–1,2-dihydrodiol and BA–3,4-dihydrodiol, participates in carcinogenesis.

Acknowledgment. This work was partly supported by Grants-in-Aid for Scientific Research from the Ministry of Education, Science, Sports and Culture of Japan.

References

(1) Yu, D., Berlin, J. A., Penning, T. M., and Field, J. (2002) Reactive oxygen species generated by PAH o-quinones cause change-in-function mutations in p53. *Chem. Res. Toxicol. 15*, 832–842.
(2) IARC Working Group (1983) General remarks. IARC monographs on the evaluation of the carcinogenic risk of chemicals to human. *Polynuclear Aromatic Compounds*, Part 1, Vol. 32, pp 33–91, IARC, Lyon.
(3) Mastrangelo, G., Fadda, E., and Marzia, V. (1996) Polycyclic aromatic hydrocarbons and cancer in man. *Environ. Health Perspect. 104*, 1166–1170.
(4) Hecht, S. S. (1999) Tobacco smoke carcinogens and lung cancer. *J. Natl. Cancer Inst. 91*, 1194–1210.
(5) IARC Working Group (1973) Benz[a]anthracene. IARC monographs on the evolution of the carcinogenic risk of chemicals to human. *Certain Polycyclic Aromatic Hydrocarbons and Heterocyclic Compounds*, Vol. 3, p 45, IARC, Lyon.
(6) Sahali, Y., Kidd, L. R., Skipper, P. L., and Tannenbaum, S. R. (1994) Metabolism of benz[a]anthracene by human liver microsomes. *Cancer Lett. 83*, 299–303.
(7) Deshiyashiki, Y., Takatsuji, T., and Hara, A. (2003) Molecular cloning and characterization of dihydrodiol dehydrogenase from the mouse. In *Aldo-Keto Reductases and Toxicant Metabolism* (Penning, T. M., and Petrash, J. M., Eds.), Chapter 7, pp 101–114, American Chemical Society, Washington, DC.
(8) Chen, C. Y., Hsu, C. P., Hsu, N. Y., Shih, C. S., Lin, T. Y., and Chow, K. C. (2002) Expression of dihydrodiol dehydrogenase in the resected stage I nonsmall cell lung cancer. *Oncol. Rep. 9*, 515–519.
(9) Yang, M. D., Wu, C. C., Chiou, S. H., Chiu, C. F., Lin, T. Y., Chiang, I. P., and Chow, K. C. (2003) Reduction of dihydrodiol dehydrogenase expression in resected hepatocellular carcinoma. *Oncol. Rep. 10*, 271–276.
(10) Chumakov, P. (1990) EMBL Data Library, accession number X54156.
(11) Yamashita, N., Murata, M., Inoue, S., Hiraku, Y., Yoshinaga, T., and Kawanishi, S. (1998) Superoxide formation and DNA damage induced by a fragrant furanone in the presence of copper(II). *Mutat. Res. 397*, 191–201.
(12) Yamamoto, K., and Kawanishi, S. (1991) Site-specific DNA damage induced by hydrazine in the presence of manganese and copper ions; the role of hydroxyl radical and hydrogen atom. *J. Biol. Chem. 266*, 1509–1515.
(13) Maxam, A. M., and Gilbert, W. (1980) Sequencing end-labeled DNA with base-specific chemical cleavages. *Methods Enzymol. 65*, 499–560.
(14) Ito, K., Inoue, S., Yamamoto, K., and Kawanishi, S. (1993) 8-Hydroxy-deoxyguanosine formation at the 5′ site of 5′-GG-3′ sequences in double-stranded DNA by UV radiation with riboflavin. *J. Biol. Chem. 268*, 13221–13227.
(15) Denissenko, M. F., Pao, A., Tang, M., and Pfeifer, G. P. (1996) Preferential formation of benzo[a]pyrene adducts at lung cancer mutational hotspots in *p53*. *Science 274*, 430–432.
(16) Ohnishi, S., and Kawanishi, S. (2002) Double base lesions of DNA by a metabolite of carcinogenic benzo[a]pyrene. *Biochem. Biophys. Res. Commun. 290*, 778–782.
(17) Flowers, L., Bleczinski, W. F., Burczynski, M. E., Harvey, R. G., and Penning, T. M. (1996) Disposition and biological activity of benzo[a]pyrene-7,8-dione. A genotoxic metabolite generated by dihydrodiol dehydrogenase. *Biochemistry 35*, 13664–13672.
(18) Palackal, N. T., Burczynski, M. E., Harvey, R. G., and Penning, T. M. (2001) The ubiquitous aldehyde reductase (AKR1A1) oxidizes proximate carcinogen *trans*-dihydrodiols to o-quinones: potential role in polycyclic aromatic hydrocarbon activation. *Biochemistry 40*, 10901–10910.
(19) Penning, T. M., Burczynski, M. E., Hung, C. F., McCoull, K. D., Palackal, N. T., and Tsuruda, L. S. (1999) Dihydrodiol dehydrogenases and polycyclic aromatic hydrocarbon activation: Generation of reactive and redox active o-quinones. *Chem. Res. Toxicol. 12*, 1–18.
(20) Hirakawa, K., Oikawa, S., Hiraku, Y., Hirosawa, I., and Kawanishi, S. (2002) Catechol and hydroquinone have different redox properties responsible for their differential DNA-damage ability. *Chem. Res. Toxicol. 15*, 76–86.
(21) Bolton, J. L., Trush, M. A., Penning, T. M., Dryhurst, G., and Monks, T. J. (2000) Role of quinones in toxicology. *Chem. Res. Toxicol. 13*, 135–160.
(22) Seike, K., Murata, M., Oikawa, S., Hiraku, Y., Hirakawa, K., and Kawanishi, S. (2003) Oxidative DNA damage induced by benz[a]anthracene metabolites via redox cycles of quinone and unique nonquinone. *Chem. Res. Toxicol. 11*, 1470–1476.

TX0498814

Available online at www.sciencedirect.com
SCIENCE DIRECT®
Nitric Oxide 11 (2004) 175–183
NITRIC OXIDE Biology and Chemistry
www.elsevier.com/locate/yniox

Mechanism of NO-mediated oxidative and nitrative DNA damage in hamsters infected with *Opisthorchis viverrini*: a model of inflammation-mediated carcinogenesis

Somchai Pinlaor[a,c,f], Yusuke Hiraku[a], Ning Ma[b], Puangrat Yongvanit[c,f], Reiji Semba[b], Shinji Oikawa[a], Mariko Murata[a], Banchob Sripa[d,f], Paiboon Sithithaworn[e,f], Shosuke Kawanishi[a,*]

[a] *Department of Environmental and Molecular Medicine, Mie University School of Medicine, Mie 514-8507, Japan*
[b] *Department of Anatomy, Mie University School of Medicine, Mie 514-8507, Japan*
[c] *Department of Biochemistry, Faculty of Medicine, Khon Kaen University, Khon Kaen 40002, Thailand*
[d] *Department of Pathology, Faculty of Medicine, Khon Kaen University, Khon Kaen 40002, Thailand*
[e] *Department of Parasitology, Faculty of Medicine, Khon Kaen University, Khon Kaen 40002, Thailand*
[f] *Liver Fluke and Cholangiocarcinoma Research Center, Faculty of Medicine, Khon Kaen University, Khon Kaen 40002, Thailand*

Received 29 March 2004; revised 22 July 2004
Available online 18 September 2004

Abstract

Inflammation mediated by infection is an important factor causing carcinogenesis. *Opisthorchis viverrini* (OV) infection is a risk factor of cholangiocarcinoma (CHCA), probably through chronic inflammation. Formation of 8-nitroguanine and 8-oxo-7,8-dihydro-2′-deoxyguanosine (8-oxodG), and expression of inducible nitric oxide synthase (iNOS) and heme oxygenase-1 (HO-1) were assessed in the liver of hamsters infected with OV. We newly produced specific anti-8-nitroguanine antibody without cross-reaction. Double immunofluorescence staining revealed that 8-oxodG and 8-nitroguanine were formed mainly in the same inflammatory cells and epithelium of bile ducts from day 7 and showed the strongest immunoreactivity on days 21 and 30, respectively. It is noteworthy that 8-oxodG and 8-nitroguanine still remained in epithelium of bile ducts on day 180, although amount of alanine aminotransferase activity returned to normal level. A time course of 8-nitroguanine was associated with iNOS expression. Furthermore, this study demonstrated that HO-1 expression and subsequent iron accumulation may be involved in enhancement of oxidative DNA damage in epithelium of small bile ducts. In conclusion, nitrative and oxidative DNA damage via iNOS expression in hamsters infected with OV may participate in CHCA carcinogenesis.

Keywords: 8-Nitroguanine; 8-Oxo-7; 8-dihydro-2′-deoxyguanosine; Heme oxygenase-1; *Opisthorchis viverrini*; Cholangiocarcinoma

Inflammation mediated by infection is an important factor causing cancer. Reactive oxygen and nitrogen species are considered to play the key role in inflammation-mediated carcinogenesis. Excess nitric oxide (NO)[1] production from inflammatory cells plays a critical role in an enormous variety of pathological processes including cancer [1,2]. Overproduction of NO leads to generation of various reactive nitrogen species, such as NO_x

* Corresponding author. Fax: +81 59 231 5011.
E-mail address: kawanisi@doc.medic.mie-u.ac.jp (S. Kawanishi).

[1] *Abbreviations used:* NO, nitric oxide; $ONOO^-$, peroxynitrite; OV, *Opisthorchis viverrini*; CHCA, cholangiocarcinoma; HO-1, heme oxygenase-1; CO, carbon monoxide; iNOS, inducible nitric oxide synthase; RSA, rabbit serum albumin; 8-oxodG, 8-oxo-7,8-dihydro-2′-deoxyguanosine; ALT, alanine aminotransferase; $O_2^{\cdot-}$ superoxide anion radical; ·OH, free hydroxyl radical; H_2O_2, hydrogen peroxide; EPO, eosinophil peroxidase.

1089-8603/$ - see front matter © 2004 Elsevier Inc. All rights reserved.
doi:10.1016/j.niox.2004.08.004

and peroxynitrite ($ONOO^-$) [3]. Reactive nitrogen species can mediate the formation of 8-nitroguanine, a marker of nitrative DNA damage [4], which has been proposed to account for infection-associated carcinogenesis [1]. Recently, Akaike et al. [5] have demonstrated the close association of 8-nitroguanosine formation with NO production in mice with viral pneumonia. Moreover, reactive nitrogen species can induce the formation of 8-oxo-7,8-dihydro-2′-deoxyguanosine (8-oxodG), which is an indicator of oxidative DNA damage [1,6,7] and a mutagenic lesion [8]. 8-Nitroguanine formed in DNA is extremely unstable, and thus depurination occurs, resulting in the formation of an apurinic site [9]. Thus, 8-nitroguanine is a putative mutagenic lesion.

Opisthorchis viverrini (OV) infection is a high risk factor of cholangiocarcinoma (CHCA) [10]. Although CHCA is a relatively rare cancer in worldwide, the highest proportional incidence rate is observed in north-east region of Thailand where the prevalence of infection with OV is also highest [10,11]. OV infection causes inflammation of the biliary epithelium, which appears to be similar in both humans and animal models [10]. In the chronic stage, the bile ducts show goblet cell metaplasia, adenomatous hyperplasia, and thickening of the walls. Complication may include biliary cirrhosis and cholangitis, and these proliferative responses are associated with the accumulation of inflammatory cells [10,12]. High levels of nitrate and nitrite reflect endogenous generation of NO resulting from OV infection in humans [13] and animals [14]. However, the mechanisms of carcinogenesis in relation to inflammation triggered by OV have not been fully elucidated.

NO regulates expression of heme oxygenase-1 (HO-1) [15–18], which is considered to play a cytoprotective role against oxidative stress [19]. HO-1 catalyzes the conversion of heme to carbon monoxide (CO), iron and biliverdin, which is immediately reduced to bilirubin [20]. Since increased CO production can induce bile canaliculi alteration [21], which may lead to cholestasis [22] and subsequent cholangitis [23], HO-1 may participate in CHCA development. Primary sclerosing cholangitis is a chronic disease, characterized by inflammation, destruction, and fibrosis of bile ducts and is an important risk factor for CHCA development [24,25]. Relevantly, cholangitis, obstructive jaundice, and hyperbilirubinemia are common complications of opisthorchiasis caused by OV infection [26].

To approach the clarification of mechanisms of CHCA development by OV infection, we focused on NO-mediated oxidative and nitrative DNA damage in the liver of hamsters by double immunofluorescence staining. Hamsters are susceptible to OV infection and suitable model of inflammation-mediated carcinogenesis. Time profile of inducible nitric oxide synthase (iNOS) expression was assessed by immunohistochemical techniques. We produced specific anti-8-nitroguanine antibody using 8-nitroguanine-aldehyde–rabbit serum albumin (RSA) conjugate and first examined 8-oxodG and 8-nitroguanine formation by double immunofluorescence technique. We also examined HO-1 expression and iron accumulation.

Experimental procedures

Chemicals and materials

8-Nitroguanine was purchased from Biolog Life Science Institute (Bremen, Germany). Mouse monoclonal anti-8-oxodG antibody was purchased from Japan Institute for the Control of Aging (Fukuroi, Japan). Rabbit polyclonal anti-iNOS and anti-HO-1 antibodies were purchased from Calbiochem–Novabiochem (Darmstadt, Germany) and Stressgen Biotechnologies (Victoria, BC, Canada), respectively. Alexa 594-labeled goat antibody against rabbit IgG and Alexa 488-labeled goat antibody against mouse IgG were obtained from Molecular Probes (Eugene, Oregon, USA). We purchased a cellulofine GCL-2000m column from Seikagaku Kogyo, Tokyo, Japan.

Parasites

Metacercariae of OV were obtained from naturally infected cyprinoid fish from an endemic area in Khon Kaen Province, Thailand. Cysts of OV were collected and identified under a dissecting microscope as described previously [27].

Animals and experimental design

Animal experiments were conducted according to the guideline of the National Committee of Animal Ethics. This study was approved by the Animal Ethic Committee of the Faculty of Medicine, Khon Kaen University, Thailand (permission No. AE003/2002). One hundred and four male Syrian golden hamsters (Animal Unit, Faculty of Medicine, Khon Kaen University) age ranging 6–8 weeks were housed under conventional conditions, and fed with a stock diet and water ad libitum. Eight groups of seven OV-infected hamsters were fed with 50 metacercariae of OV by intragastric intubation, while six non-infected hamsters were fed with saline solution at the same route. Days 3, 7, 14, 21, and 30 were defined as the early phase, and days 60, 90, and 180 were defined as the late phase according to our results.

Liver function enzyme activity assay

Plasma alanine aminotransferase (ALT) activity was analyzed by a spectrophotometer (automate RA100)

using a commercial kit (Thermo Trace Ltd., Australia). Conformance biochemistry control was used as the standard of this enzyme.

Production of anti-8-nitroguanine antibody

Anti-8-nitroguanine polyclonal antibody was produced by a modified method [28]. 8-Nitroguanosine was incubated with sodium metaperiodate for 20 min at room temperature and then conjugated with RSA for 1 h followed by incubation with sodium borohydride for 1 h. The conjugate was dialyzed against 150 mM NaCl overnight. 8-Nitroguanine–aldehyde–RSA conjugate mixed with Freund's complete adjuvant was injected in rabbit by intracutaneous administration. After 4 weeks of the immunization, the same antigen was given and the blood was taken 10 days later. We immobilized 8-nitroguanine in a cellulofine GCL-2000m column (Seikagaku Kogyo), and then purified the antibody by affinity chromatography. Specificity of the purified antibody was examined by a dot immunobinding assay and absorption test [29].

Double immunofluorescence staining of 8-nitroguanine and 8-oxodG

Double immunofluorescence labeling studies of 8-nitroguanine and 8-oxodG in the hamster livers were performed as described previously [30]. Briefly, paraffin sections (6-μm thickness) were deparaffinized and microwaved in 5% urea for 5 min twice. The sections were incubated with 1% skim milk for 30 min. Then, the sections were incubated with rabbit polyclonal anti-8-nitroguanine antibody (2 μg/ml) and mouse monoclonal anti-8-oxodG antibody (5 μg/ml) overnight at room temperature. Finally, they were incubated with Alexa 594-labeled goat antibody against rabbit IgG and Alexa 488-labeled goat antibody against mouse IgG (1:400) for 3 h. The immunostained sections were examined under an invert Laser Scan Microscope (LSM 410, Zeiss, Gottingen, Germany).

Immunohistochemical study of iNOS and HO-1 expression

iNOS and HO-1 expression in the liver of hamsters infected with OV was performed by indirect immunofluorescence technique as described previously [31]. The sections were incubated with rabbit polyclonal anti-iNOS antibody (1:500) or anti-HO-1 antibody (1:500) followed by incubation with Alexa 594-labeled goat antibody against rabbit IgG (1:400) and analyzed by using a Laser Scan Microscope. In certain experiments, immunohistochemical analysis for HO-1 was carried out using goat anti-rabbit IgG-HRP (1:200). Sections are visualized with 3,3-diaminobenzidine tetrahydrochloride as chromogen.

Histopathological study and iron staining

Histopathological study was performed by hematoxylin and eosin staining in paraffin sections as described previously [27]. Accumulation of iron in the liver tissue was examined by Prussian blue method in paraffin sections. This method was employed to stain ferric iron as described previously [32].

Statistical analysis

The Student's t test was used to compare infected and non-infected samples and a value of $P < 0.05$ was considered significant.

Results

Change of ALT activity in OV-infected hamsters

Fig. 1 shows the changes of plasma ALT activity. ALT activity in infected hamsters was significantly higher than that in control hamsters from day 14 ($P < 0.01$) and reached the highest peak on day 21 ($P < 0.001$). Then ALT activity was rapidly decreased on day 30, but remained at higher level than that of normal hamster until day 90 ($P < 0.001$).

Specificity of anti-8-nitroguanine antibody

Purified antibody gave a strong immunostaining only on the spot of 8-nitroguanine conjugate (Fig. 2A). The immunoreactivity disappeared only when the antibody was preincubated with 8-nitroguanine (Fig. 2B). In contrast, immunoreactivity with 8-nitroguanine conjugate

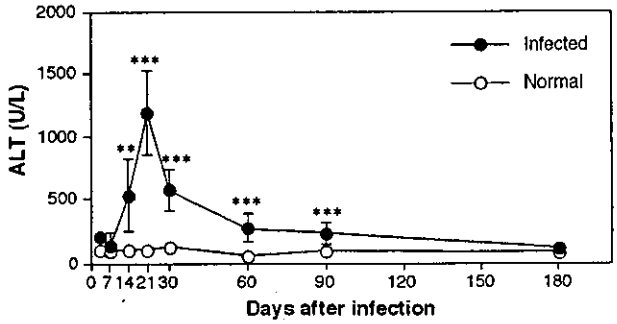

Fig. 1. Change of ALT activity in OV-infected hamsters. Plasma ALT activity was determined as described in Experimental procedures. The data were presented in means ± SD. The Student's t test was used to compare seven infected and six non-infected samples. $^{**}P < 0.01$ and $^{***}P < 0.001$.

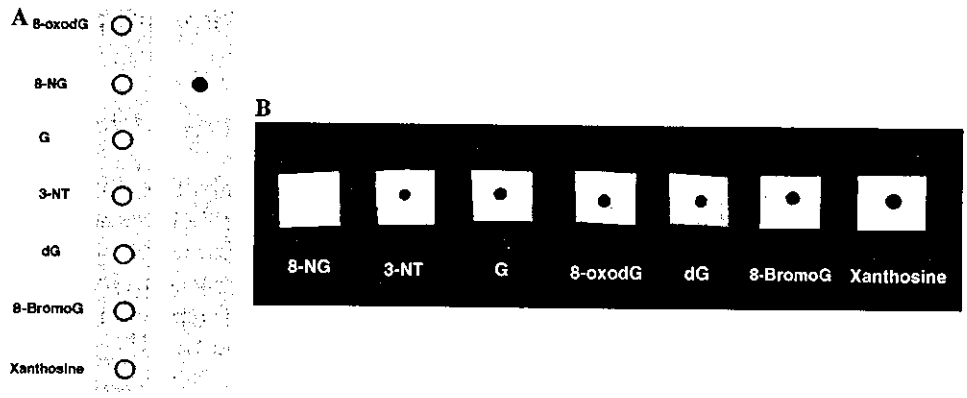

Fig. 2. Dot immunobinding assay and absorption test of anti-8-nitroguanine antibody. Antigen–antibody reactions were visualized by the peroxidase-anti-peroxidase method. Purified antibody gave a strong immunostaining only on the spot of 8-nitroguanine conjugate (A). 8-Nitroguanine, 3-nitrotyrosine, guanosine, 8-oxodG, and deoxyguanosine were incubated with the antibody at the concentration of 0.7 μg/ml, and were applied to 8-nitroguanine conjugate. Immunoreactivity disappeared only when the antibody was pretreated with 8-nitroguanine (B). 8-NG, 8-nitroguanine; 3-NT, 3-nitrotyrosine; G, guanosine; dG, deoxyguanosine; and 8-BromoG, 8-bromoguanosine.

did not disappear when the antibody was preincubated with 3-nitrotyrosine, guanosine, 8-oxodG, deoxyguanosine, 8-bromoguanosine, and xanthosine (Fig. 2B).

8-oxodG and 8-nitroguanine formation in the liver of hamsters infected with OV

A time profile of 8-oxodG and 8-nitroguanine formation in the liver of hamsters infected with OV was assessed by double immunofluorescence staining. Anti-8-nitroguanine antibody gave a strong and specific immunostaining at a low concentration of 2 μg/ml. 8-oxodG and 8-nitroguanine immunoreactivity was not observed in the liver of normal hamsters (Fig. 3, normal). In the early phase, both 8-oxodG and 8-nitroguanine formation was observed mainly in the nucleus of the same small inflammatory cells (Fig. 3, 30D (inset)) and in epithelium of bile ducts (Fig. 3, 21D) from day 7. A marked increase in the number of intensely 8-oxodG and 8-nitroguanine immunoreactive cells was seen from day 14 and the number was the largest on days 21 and 30, respectively. Some large inflammatory cells, in which only 8-oxodG was formed in the cytoplasm, appeared from day 14 (Fig. 3, 14D). In the late phase, the number of inflammatory cells, in which both 8-oxodG and 8-nitroguanine were stained in the nucleus, decreased on days 90 and 180. Interestingly, 8-oxodG and 8-nitroguanine were formed in some small bile ducts on day 180 (Fig. 3, 180D (arrow)). The immunoreactivity of 8-oxodG was observed mainly in the cytoplasm and partially in the nucleus of predominating large inflammatory cells and small bile ducts (Fig. 3, 180D). In contrast, 8-oxodG and 8-nitroguanine formation was scarcely observed in hepatocytes.

iNOS expression in the liver of hamsters infected with OV

iNOS immunoreactivity was not observed in the liver from normal hamsters (Fig. 4, normal). Weak iNOS immunoreactivity was found in inflammatory cells on day 3 (Fig. 4, 3D). iNOS immunoreactivity was observed only in the cytoplasm of inflammatory cells (Fig. 4, 21D (inset)) and epithelium of bile ducts (Fig. 4, 7D, 14D, and 90D (inset a)). The number of these intensely immunoreactive cells was the largest on day 30 and decreased on day 90. iNOS expression was also observed in small bile ducts on days 90 and 180 (Fig. 4, 90D (inset b) and 180D). iNOS expression was weakly found in hepatocytes (Fig. 4, 7D inset).

HO-1 expression in the liver of hamsters infected with OV

HO-1 expression was not observed in the liver from normal hamsters (Fig. 5, normal). Intense HO-1 immunoreactivity was observed in epithelium of bile ducts from day 7. Intense immunoreactivity of HO-1 was observed in cells in the sinusoid (Fig. 5, 14D, inset and "HE + HO-1"), suggesting that HO-1 is expressed specifically in Kupffer cells. The intensity of HO-1 immunoreactivity in inflammatory cells was the highest on day 30 and then decreased on days 90 and 180. Interestingly, HO-1 expression was mainly found in epithelium of bile ducts on day 90 (Fig. 5, 90D) as well as in small bile ducts on day 180 (Fig. 5, 180D). In contrast, no HO-1 expression was found in hepatocytes.

Histopathological changes and iron accumulation in the liver of hamsters infected with OV

Histopathological study showed that accumulation of bile pigment and formation of small bile ducts were

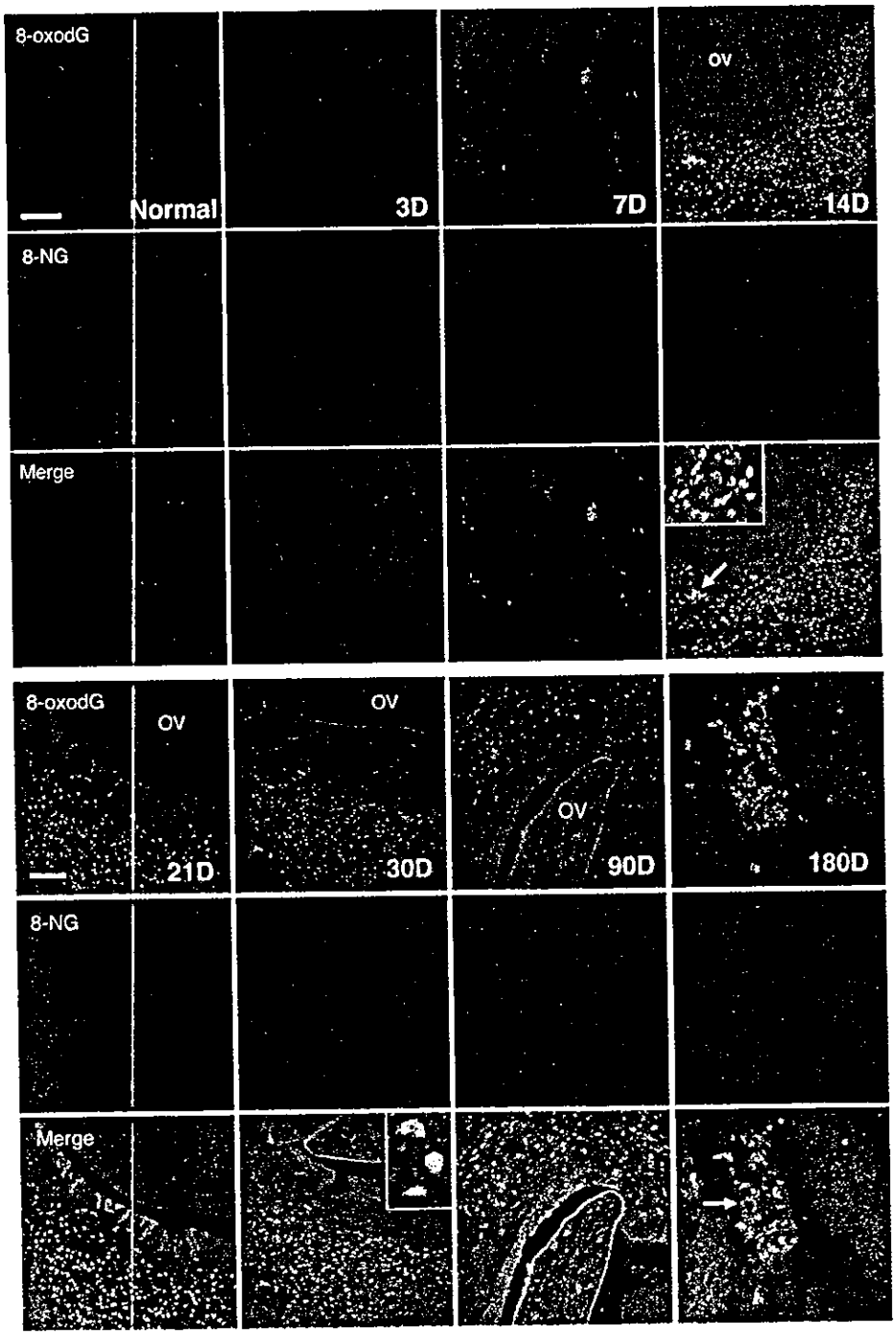

Fig. 3. Double immunofluorescence staining of 8-oxodG and 8-nitroguanine in the liver of OV-infected hamsters. Immunoreactivity of both 8-oxodG and 8-nitroguanine was observed mostly in the same inflammatory cells and epithelium of bile ducts (14D (inset), 21D, 30D (inset), and 180D (arrow)). The staining intensity of 8-oxodG and 8-nitroguanine was highest on days 21 and 30, respectively. Only intense 8-oxodG immunoreactivity was observed in some multinuclear giant cells (14D (arrow)) and large inflammatory cells (90D and 180D). 8-NG, 8-nitroguanine, bar = 50 μm.

frequently found on days 90 and 180, respectively (data not shown). These histopathological changes in the liver of hamsters infected with OV in the present study were similar to the previous reports [12,27].

Little or no iron was observed in normal liver (Fig. 6, normal). In the early phase, iron began to be widely distributed in hepatocytes and Kupffer cells at inflammatory areas from day 7 and was markedly observed on day 14 (Fig. 6, 14D). Iron deposition was observed around the large bile ducts on days 21 and 30 (Fig. 6, 30D). HO-1 expression was observed in bile duct epithelial cells, and iron deposition was seen around bile duct. This observation suggests that iron deposition is mediated by HO-1 during OV infection. Notably, the largest

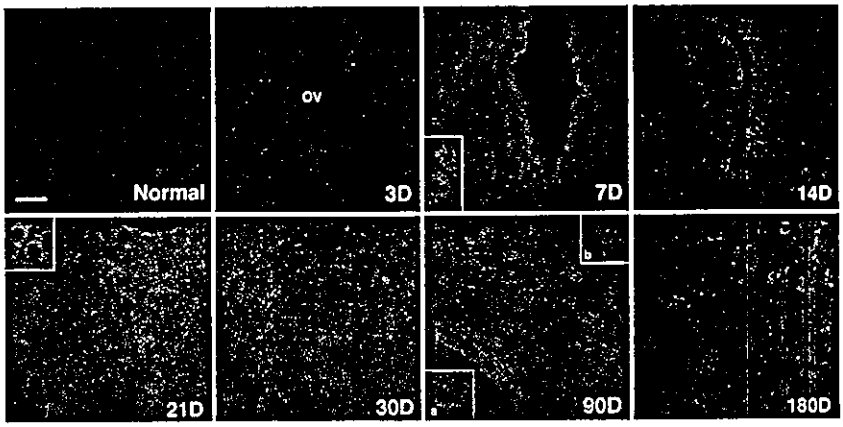

Fig. 4. Alteration of iNOS expression in the liver of hamsters infected with OV. iNOS expression was analyzed by immunohistochemical technique as described in Experimental procedures. The number of intensely immunoreactive inflammatory cells and epithelium of bile ducts was the largest on day 30 and decreased on days 90 and 180. iNOS expression was also observed in small bile ducts (90D (inset b) and 180D). iNOS expression was observed mainly in the cytoplasm of inflammatory cells (21D (inset)) and epithelium of bile ducts (90D (inset a)). Weak immunoreactivity was found in hepatocytes (7D (inset)) and OV. Bar = 50 μm.

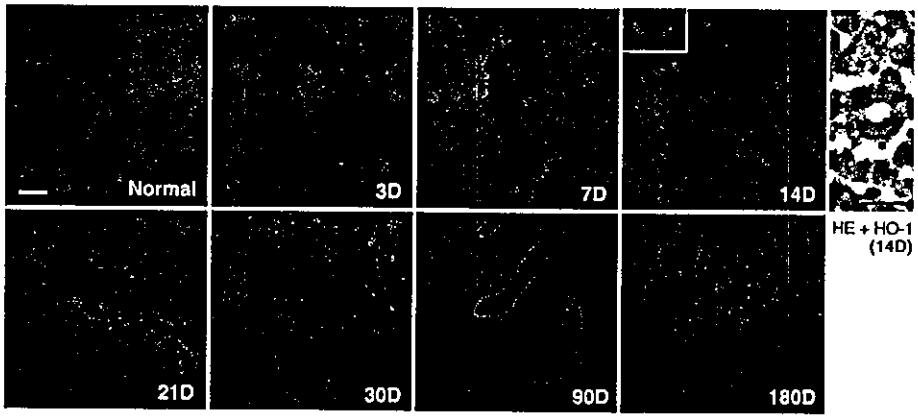

Fig. 5. Time course of HO-1 expression in the liver of OV-infected hamsters. HO-1 expression was analyzed by immunohistochemical technique as described in Experimental procedures. Immunoreactivity of HO-1 was markedly observed in Kupffer cells (14D (inset) and HE + HO-1). The immunoreactivity of epithelium of bile ducts and inflammatory cells was observed from day 7 and the highest on day 30 (30D). HO-1 expression was also observed in small bile ducts (90D and 180D). HE + HO-1, hematoxylin and eosin staining, and immunohistochemistry for HO-1 expression with goat anti-rabbit IgG-HRP were performed in the same slide (day 14). Bar = 50 μm.

accumulation of iron was found around small bile ducts on day 180 (Fig. 6, 180D).

Discussion

This study shows that iNOS expression mediates the simultaneous formation of 8-oxodG and 8-nitroguanine in the nucleus of same inflammatory cells and epithelium of bile ducts in the early phase. Relevantly, Jaiswal et al. [33] have demonstrated that iNOS expression mediates 8-oxodG formation in cultured CHCA cells. In the late phase, both 8-oxodG and 8-nitroguanine were mostly observed in small inflammatory cells, bile duct epithelium and small bile ducts. OV infection induced iNOS expression, followed by HO-1 expression in Kupffer cells and bile ducts and subsequent accumulation of iron around bile ducts.

In the early phase, 8-oxodG and 8-nitroguanine formation reached the maximal level on days 21 and 30, respectively. The previous study showed that a time profile of 8-oxodG formation was closely associated with eosinophil infiltration, whereas 8-nitroguanine formation was associated with mononuclear cell infiltration [31]. In this study, 8-nitroguanine formation was associated with iNOS expression. OV antigen is considered to induce eosinophil migration and subsequent mononuclear cell infiltration in portal areas [27,34]. Superoxide anion radical ($O_2^{\cdot-}$) is generated from eosinophils [34] and macrophages [35]. $O_2^{\cdot-}$ is spontaneously dismutated into hydrogen peroxide (H_2O_2), and then activated by metal ions such as Fe^{2+} or Cu^{+} to form free hydroxyl radical ($^{\cdot}OH$) or metal-hydroperoxide [3,7]. These reactive oxygen species lead to oxidation of DNA bases such as 8-oxodG formation [7]. This immunohistochemical study supports the idea that mononuclear cells, includ-

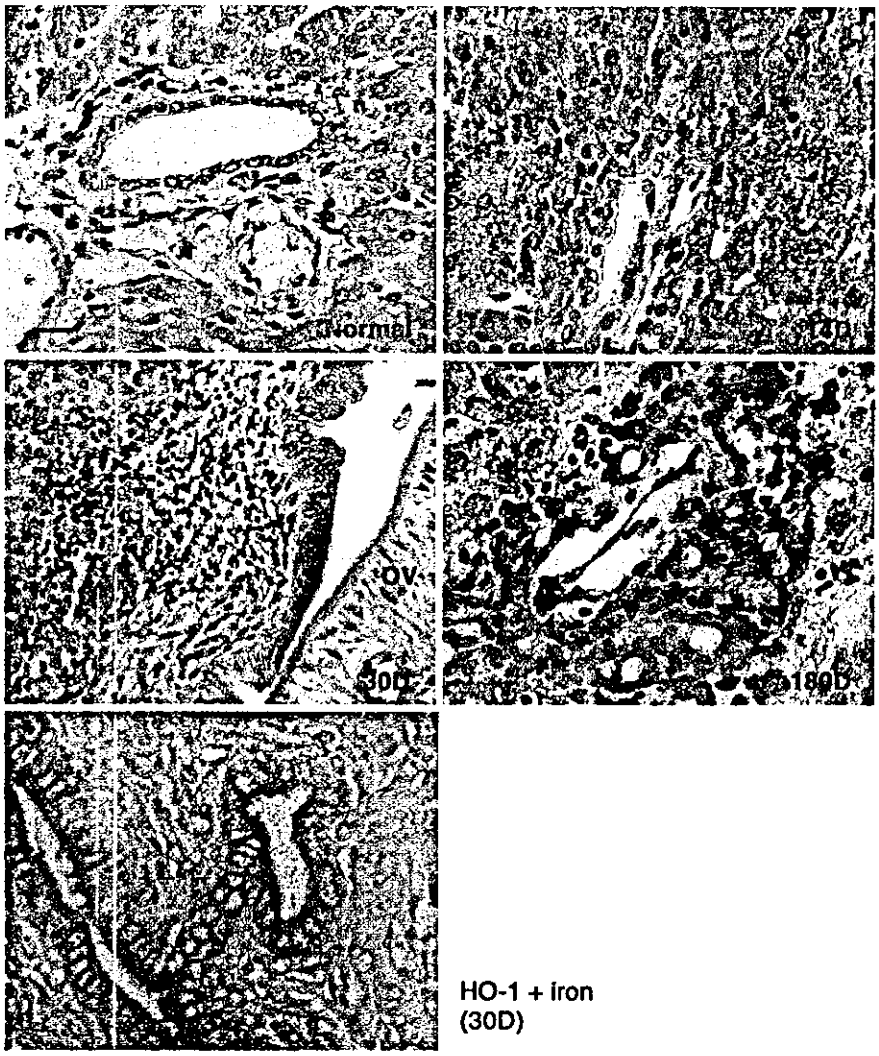

Fig. 6. Iron deposition in the liver of hamsters infected with OV. Iron was stained by Prussian blue method in paraffin sections as described in Experimental procedures. Iron was widely distributed at inflammatory areas (14D). Iron deposition was observed around large bile ducts (30D and HO-1 + iron) and small bile ducts (180D). HO-1 is expressed in bile duct epithelial cells (HO-1 + iron). Normal, 14D and 180D, bar = 100 μm; 30D, bar = 50 μm. HO-1 + iron, immunohistochemistry for HO-1 expression with goat anti-rabbit IgG-HRP and iron staining were performed in the same slide (day 30).

ing macrophages and lymphocytes, generate mainly NO [36]. NO is also derived from eosinophils [37] and rapidly reacts with $O_2^{\bullet-}$ to form $ONOO^-$, and then induces 8-oxodG [6,38] and 8-nitroguanine formation [4,39]. Moreover, activation of eosinophil peroxidase (EPO) is characteristic for parasitic infections [40]. Myeloperoxidase and EPO in the presence of H_2O_2 and nitrite can also catalytically generate reactive nitrogen dioxide, which can form 8-nitroguanine [41]. Collectively, NO and additional $O_2^{\bullet-}$ production mediates 8-oxodG and 8-nitroguanine formation mainly in nuclear DNA in the same inflammatory cells and epithelium of bile ducts in the liver of hamsters infected with OV.

We observed that iNOS was expressed in bile duct epithelium from the early phase and its expression continued in the late phase. Interestingly, in the late phase, iNOS expression was still observed in small bile ducts on day 180. Concomitantly, 8-oxodG and 8-nitroguanine were formed in the same cells on days 90 and 180. These results suggest that iNOS expression plays an important role in carcinogenesis through 8-oxodG and 8-nitroguanine formation. It is noteworthy that although ALT activity trended to normal level on day 180, nucleic acid damage, especially 8-oxodG, still remained in epithelium of bile ducts. Sustainable formation of 8-oxodG and separate localization of 8-oxodG and 8-nitroguanine may be explained by the report that lipid peroxidation products cause additional 8-oxodG formation in human DNA [42]. The formation of 8-oxodG in the cytoplasm in the late phase may be explained by assuming that 8-oxodG can be formed in mitochondrial DNA [43]. 8-Nitroguanine and 8-oxodG formation in DNA is known

to cause mutation, leading to carcinogenesis. 8-oxodG formation results in G:C to T:A transversion, which is frequently found in tumor relevant genes [1,8]. 8-Nitroguanine undergoes spontaneous depurination leading to apurinic sites in DNA [9], resulting in G:C to T:A transversion [1,9]. Thamavit et al. [44] have shown that OV infection has a potential to cause cholangiocarcinoma in hamsters. We believe that in addition to 8-oxodG formation, accumulation of 8-nitroguanine may participate in liver fluke-induced mutation in the initiation and/or promotion steps of carcinogenesis.

In the present study, iNOS expression was followed by HO-1 expression from day 7. This result suggests that NO mediates HO-1 expression in the liver of hamsters infected with OV. This finding is supported by recent reports showing that NO is capable of inducing HO-1 expression in cultured cells [15–18]. We also observed HO-1 expression in not only Kupffer cells but also epithelium of bile ducts and small bile duct, although Kupffer cell-specific induction of HO-1 is well established in liver injury [45]. Expression of HO-1 generates CO, iron, and biliverdin, which is immediately reduced to bilirubin [20]. It is generally accepted that bilirubin is an antioxidant, and HO-1 expression may participate in protection against oxidative stress. This study showed that HO-1 was expressed in bile duct epithelial cells, followed by iron deposition around bile duct. Iron is a risk factor for certain types of cancer via the formation of reactive oxygen species [46,47]. Notably, our observation suggests that HO-1-mediated iron deposition during OV infection may be involved in enhancement of oxidative DNA damage. Whysner and Wang [32] have demonstrated that iron accumulation increases liver cell proliferation and the development of hepatocarcinogenesis. Thus, iron deposition at inflammatory areas and around large and small bile ducts via HO-1 expression may participate in carcinogenesis.

It can be concluded that nitrative and oxidative DNA damage via iNOS expression in hamsters infected with OV participates in CHCA carcinogenesis. Furthermore, NO may be involved in carcinogenesis through HO-1-derived iron accumulation, leading to enhancement of oxidative DNA damage in the epithelium of small bile ducts. 8-oxodG and 8-nitroguanine detected by double immunofluorescence staining could be potential biomarkers to evaluate the risk of inflammation-related carcinogenesis.

Acknowledgments

This work was supported by Khon Kaen Research Fund in Thailand and Grants-in-Aid for Scientific Research from the Ministry of Education, Science, Sports and Culture of Japan.

References

[1] H. Ohshima, M. Tatemichi, T. Sawa, Chemical basis of inflammation-induced carcinogenesis, Arch. Biochem. Biophys. 417 (2003) 3–11.
[2] S.P. Hussain, L.J. Hofseth, C.C. Harris, Radical causes of cancer, Nat. Rev. Cancer 3 (2003) 276–285.
[3] B. Halliwell, Oxygen and nitrogen are pro-carcinogens. Damage to DNA by reactive oxygen, chlorine and nitrogen species: measurement, mechanism and the effects of nutrition, Mutat. Res. 443 (1999) 37–52.
[4] V. Yermilov, J. Rubio, M. Becchi, M.D. Friesen, B. Pignatelli, H. Ohshima, Formation of 8-nitroguanine by the reaction of guanine with peroxynitrite in vitro, Carcinogenesis 16 (1995) 2045–2050.
[5] T. Akaike, S. Okamoto, T. Sawa, J. Yoshitake, F. Tamura, K. Ichimori, K. Miyazaki, K. Sasamoto, H. Maeda, 8-Nitroguanosine formation in viral pneumonia and its implication for pathogenesis, Proc. Natl. Acad. Sci. USA 100 (2003) 685–690.
[6] J.P. Spencer, J. Wong, A. Jenner, O.I. Aruoma, C.E. Cross, B. Halliwell, Base modification and strand breakage in isolated calf thymus DNA and in DNA from human skin epidermal keratinocytes exposed to peroxynitrite or 3-morpholinosydnonimine, Chem. Res. Toxicol. 9 (1996) 1152–1158.
[7] S. Kawanishi, Y. Hiraku, S. Oikawa, Mechanism of guanine-specific DNA damage by oxidative stress and its role in carcinogenesis and aging, Mutat. Res. 488 (2001) 65–76.
[8] S.D. Bruner, D.P. Norman, G.L. Verdine, Structural basis for recognition and repair of the endogenous mutagen 8-oxoguanine in DNA, Nature 403 (2000) 859–866.
[9] L.A. Loeb, B.D. Preston, Mutagenesis by apurinic/apyrimidinic sites, Annu. Rev. Genet. 20 (1986) 201–230.
[10] IARC Working Group, Infection with liver flukes (*Opisthorchis viverrini*, *Opisthorchis felineus* and *Clonorchis sinensis*), IARC Monographs on the Evaluation of Carcinogenic Risks to Humans 61 (1994) 121–175.
[11] M.R. Haswell-Elkins, E. Mairiang, P. Mairiang, J. Chaiyakum, N. Chamadol, V. Loapaiboon, P. Sithithaworn, D.B. Elkins, Cross-sectional study of *Opisthorchis viverrini* infection and cholangiocarcinoma in communities within a high-risk area in northeast Thailand, Int. J. Cancer 59 (1994) 505–509.
[12] N. Bhamarapravati, W. Thammavit, S. Vajrasthira, Liver changes in hamsters infected with a liver fluke of man, *Opisthorchis viverrini*, Am. J. Trop. Med. Hyg. 27 (1978) 787–794.
[13] M.R. Haswell-Elkins, S. Satarug, M. Tsuda, E. Mairiang, H. Esumi, P. Sithithaworn, P. Mairiang, M. Saitoh, P. Yongvanit, D.B. Elkins, Liver fluke infection and cholangiocarcinoma: model of endogenous nitric oxide and extragastric nitrosation in human carcinogenesis, Mutat. Res. 305 (1994) 241–252.
[14] H. Ohshima, T.Y. Bandaletova, I. Brouet, H. Bartsch, G. Kirby, F. Ogunbiyi, V. Vatanasapt, V. Pipitgool, Increased nitrosamine and nitrate biosynthesis mediated by nitric oxide synthase induced in hamsters infected with liver fluke (*Opisthorchis viverrini*), Carcinogenesis 15 (1994) 271–275.
[15] M. Andre, E. Felley-Bosco, Heme oxygenase-1 induction by endogenous nitric oxide: influence of intracellular glutathione, FEBS Lett. 546 (2003) 223–227.
[16] C. Bouton, B. Demple, Nitric oxide-inducible expression of heme oxygenase-1 in human cells. Translation-independent stabilization of the mRNA and evidence for direct action of nitric oxide, J. Biol. Chem. 275 (2000) 32688–32693.
[17] E. Hara, K. Takahashi, K. Takeda, M. Nakayama, M. Yoshizawa, H. Fujita, K. Shirato, S. Shibahara, Induction of heme oxygenase-1 as a response in sensing the signals evoked by distinct nitric oxide donors, Biochem. Pharmacol. 58 (1999) 227–236.

[18] P. Naughton, R. Foresti, S.K. Bains, M. Hoque, C.J. Green, R. Motterlini, Induction of heme oxygenase 1 by nitrosative stress. A role for nitroxyl anion, J. Biol. Chem. 277 (2002) 40666–40674.
[19] G. Speit, C. Dennog, U. Eichhorn, A. Rothfuss, B. Kaina, Induction of heme oxygenase-1 and adaptive protection against the induction of DNA damage after hyperbaric oxygen treatment, Carcinogenesis 21 (2000) 1795–1799.
[20] F.A. Wagener, H.D. Volk, D. Willis, N.G. Abraham, M.P. Soares, G.J. Adema, C.G. Figdor, Different faces of the heme–heme oxygenase system in inflammation, Pharmacol. Rev. 55 (2003) 551–571.
[21] Y. Shinoda, M. Suematsu, Y. Wakabayashi, T. Suzuki, N. Goda, S. Saito, T. Yamaguchi, Y. Ishimura, Carbon monoxide as a regulator of bile canalicular contractility in cultured rat hepatocytes, Hepatology 28 (1998) 286–295.
[22] M. Suematsu, Y. Ishimura, The heme oxygenase-carbon monoxide system: a regulator of hepatobiliary function, Hepatology 31 (2000) 3–6.
[23] W. Thamavit, M.A. Moore, Y. Hiasa, N. Ito, Enhancement of DHPN induced hepatocellular, cholangiocellular and pancreatic carcinogenesis by *Opisthorchis viverrini* infestation in Syrian golden hamsters, Carcinogenesis 9 (1988) 1095–1098.
[24] R. Poupon, O. Chazouilleres, R.E. Poupon, Chronic cholestatic diseases, J. Hepatol. 32 (2000) 129–140.
[25] F. Holzinger, K. Z'Graggen, M.W. Buchler, Mechanisms of biliary carcinogenesis: a pathogenetic multi-stage cascade towards cholangiocarcinoma, Ann. Oncol. 10 (1999) 122–126.
[26] S. Pungpak, M. Riganti, D. Bunnag, T. Harinasuta, Clinical features in severe opisthorchiasis viverrini, Southeast Asian J. Trop. Med. Public Health 16 (1985) 405–409.
[27] B. Sripa, S. Kaewkes, Localisation of parasite antigens and inflammatory responses in experimental opisthorchiasis, Int. J. Parasitol. 30 (2000) 735–740.
[28] B.F. Erlanger, S.M. Beiser, Antibodies specific for ribonucleosides and ribonucleotides and their reaction with DNA, Proc. Natl. Acad. Sci. USA 52 (1964) 68–74.
[29] R. Hawkes, E. Niday, J. Gordon, A dot-immunobinding assay for monoclonal and other antibodies, Anal. Biochem. 119 (1982) 142–147.
[30] N. Ma, X. Ding, T. Miwa, R. Semba, Immunohistochemical localization of taurine in the rat stomach, Adv. Exp. Med. Biol. 526 (2003) 229–236.
[31] S. Pinlaor, P. Yongvanit, Y. Hiraku, N. Ma, R. Semba, S. Oikawa, M. Murata, B. Sripa, P. Sithithaworn, S. Kawanishi, 8-Nitroguanine formation in the liver of hamsters infected with *Opisthorchis viverrini*, Biochem. Biophys. Res. Commun. 309 (2003) 567–571.
[32] J. Whysner, C.X. Wang, Hepatocellular iron accumulation and increased cell proliferation in polychlorinated biphenyl-exposed Sprague–Dawley rats and the development of hepatocarcinogenesis, Toxicol. Sci. 62 (2001) 36–45.
[33] M. Jaiswal, N.F. LaRusso, L.J. Burgart, G.J. Gores, Inflammatory cytokines induce DNA damage and inhibit DNA repair in cholangiocarcinoma cells by a nitric oxide-dependent mechanism, Cancer Res. 60 (2000) 184–190.
[34] M.L. McCormick, A. Metwali, M.A. Railsback, J.V. Weinstock, B.E. Britigan, Eosinophils from schistosome-induced hepatic granulomas produce superoxide and hydroxyl radical, J. Immunol. 157 (1996) 5009–5015.
[35] M. Kato, K. Tokuyama, H. Minakami, A. Nagai, K. Kozawa, H. Goto, A. Morikawa, H. Kimura, Increased superoxide radicals generation from alveolar macrophages in immature guinea-pigs, Cell. Biol. Int. 26 (2002) 829–832.
[36] A.W. Taylor-Robinson, F.Y. Liew, A. Severn, D. Xu, S.J. McSorley, P. Garside, J. Padron, R.S. Phillips, Regulation of the immune response by nitric oxide differentially produced by T helper type 1 and T helper type 2 cells, Eur. J. Immunol. 24 (1994) 980–984.
[37] V. del Pozo, E. de Arruda-Chaves, B. de Andres, B. Cardaba, A. Lopez-Farre, S. Gallardo, I. Cortegano, L. Vidarte, A. Jurado, J. Sastre, P. Palomino, C. Lahoz, Eosinophils transcribe and translate messenger RNA for inducible nitric oxide synthase, J. Immunol. 158 (1997) 859–864.
[38] S. Inoue, S. Kawanishi, Oxidative DNA damage induced by simultaneous generation of nitric oxide and superoxide, FEBS Lett. 371 (1995) 86–88.
[39] Y.S. Hsieh, H.C. Wang, T.H. Tseng, W.C. Chang, C.J. Wang, Gaseous nitric oxide-induced 8-nitroguanine formation in human lung fibroblast cells and cell-free DNA, Toxicol. Appl. Pharmacol. 172 (2001) 210–216.
[40] W. Wu, Y. Chen, A. d'Avignon, S.L. Hazen, 3-Bromotyrosine and 3,5-dibromotyrosine are major products of protein oxidation by eosinophil peroxidase: potential markers for eosinophil-dependent tissue injury in vivo, Biochemistry 38 (1999) 3538–3548.
[41] H.J. Chen, Y.M. Chen, T.F. Wang, K.S. Wang, J. Shiea, 8-Nitroxanthine, an adduct derived from 2′-deoxyguanosine or DNA reaction with nitryl chloride, Chem. Res. Toxicol. 14 (2001) 536–546.
[42] T. Kaneko, S. Tahara, Formation of 8-oxo-2′-deoxyguanosine in the DNA of human diploid fibroblasts by treatment with linoleic acid hydroperoxide and ferric ion, Lipids 35 (2000) 961–965.
[43] R.P. Soultanakis, R.J. Melamede, I.A. Bespalov, S.S. Wallace, K.B. Beckman, B.N. Ames, D.J. Taatjes, Y.M. Janssen-Heininger, Fluorescence detection of 8-oxoguanine in nuclear and mitochondrial DNA of cultured cells using a recombinant Fab and confocal scanning laser microscopy, Free Radic. Biol. Med. 28 (2000) 987–998.
[44] W. Thamavit, M.A. Moore, S. Sirisinha, T. Shirai, N. Ito, Time-dependent modulation of liver lesion development in Opisthorchis-infected Syrian hamster by an antihelminthic drug, praziquantel, Jpn. J. Cancer Res. 84 (1993) 135–138.
[45] T. Kobayashi, K. Hirano, T. Yamamoto, G. Hasegawa, K. Hatakeyama, M. Suematsu, M. Naito, The protective role of Kupffer cells in the ischemia–reperfused rat liver, Arch. Histol. Cytol. 65 (2002) 251–261.
[46] C.W. Wu, Y.Y. Wei, C.W. Chi, W.Y. Lui, F.K. P'Eng, C. Chung, Tissue potassium, selenium, and iron levels associated with gastric cancer progression, Dig. Dis. Sci. 41 (1996) 119–125.
[47] S. Toyokuni, Iron and carcinogenesis: from Fenton reaction to target genes, Redox Rep. 7 (2002) 189–197.

Available online at www.sciencedirect.com
SCIENCE DIRECT
Biochemical Pharmacology 68 (2004) 1869–1878
Biochemical Pharmacology
www.elsevier.com/locate/biochempharm

Oxidative DNA damage induced by a melatonin metabolite, 6-hydroxymelatonin, via a unique non-*o*-quinone type of redox cycle

Katsuhisa Sakano, Shinji Oikawa, Yusuke Hiraku, Shosuke Kawanishi*

Department of Environmental and Molecular Medicine, Mie University School of Medicine, Mie 5148507, Japan

Received 19 February 2004; accepted 18 June 2004

Abstract

Melatonin, an indolic pineal hormone, is produced primarily at night in mammals and is important in controlling biological rhythms. Although melatonin is known to be effective as a free radical scavenger and has an anti-cancer effect, carcinogenic properties have also been reported. In relation to its carcinogenic potential, we have examined whether 6-hydroxymelatonin, a major melatonin metabolite, can induce DNA damage in the presence of metal ion using [^{32}P]-5′-end-labeled DNA fragments obtained from genes relevant to human cancer. 6-Hydroxymelatonin induced site-specific DNA damage in the presence of Cu(II). Formamidopyrimidine-DNA glycosylase treatment induced cleavage sites mainly at G residues of the 5′-TG-3′ sequence, whereas piperidine treatment induced cleavage sites at T mainly of 5′-TG-3′. Interestingly, 6-hydroxymelatonin strongly damaged G and C of the 5′-ACG-3′ sequence complementary to codon 273 of the *p53* gene. These results suggest that 6-hydroxymelatonin can cause double-base lesions. DNA damage was inhibited by both catalase and bathocuproine, Cu(I)-specific stabilizer, suggesting that reactive species derived from the reaction of H_2O_2 with Cu(I) participate in DNA damage. Cytochrome P450 reductase efficiently enhanced 6-hydroxymelatonin-induced oxidative DNA damage and oxygen consumption, suggesting the formation of redox cycle. It is noteworthy that 6-hydroxymelatonin can efficiently induce DNA damage via non-*o*-quinone type of redox cycle. Formation of 8-oxo-7,8-dihydro-2′-deoxyguanosine (8-oxodG), a characteristic oxidative DNA lesion, in calf thymus DNA was significantly increased by 6-hydroxymelatonin in the presence of Cu(II). Furthermore, 6-hydroxymelatonin significantly increased the formation of 8-oxodG in human leukemia cell line HL-60 but not in HP100, a hydrogen peroxide (H_2O_2)-resistant cell line derived from HL-60. The 6-hydroxymelatonin-induced 8-oxodG formation in HL-60 cells significantly decreased by the addition of bathocuproine or *o*-phenanthroline. Therefore, it is concluded that melatonin may exhibit carcinogenic potential through oxidative DNA damage by its metabolite.

Keywords: DNA damage; Melatonin; 6-Hydroxymelatonin; 8-oxodG; Copper; Hydrogen peroxide

1. Introduction

Melatonin (*N*-acetyl-5-methoxytryptamine), an indolic hormone, is clearly involved in the control of circadian and photoperiodic systems in mammals [1,2]. Melatonin was also discovered to be a direct free radical scavenger [3]. Beside its ability to neutralize a number of free radicals including reactive oxygen and nitrogen, it stimulates several antioxidative enzymes (superoxide dismutase, glutathione peroxidase, and glutathione reductase) [4,5]. It has been reported that melatonin has anti-cancer properties [6,7]. The growth of mammary and ovarian tumor cells was inhibited by physiological concentration of melatonin [8]. Some reports suppose that melatonin has a wide range of health benefits because of its reported anitoxidative properties [9–11]. More than 20 million Americans have taken melatonin supplement, frequently at high dose, over long periods and without any medical monitoring [12].

On the other hand, dietary administration of melatonin induced lymphomas and leukemias (and malignant tumor)

Abbreviations: 8-oxodG, 8-oxo-7,8-dihydro-2′-deoxyguanosine (and also known as 8-hydroxy-2′-deoxyguanosine); HPLC-ECD, an electrochemical detector coupled to a high-pressure liquid chromatography; DTPA, diethylenetriamine-*N*,*N*,*N*′,*N*′,*N*″-pentaacetic acid; $O_2^{\cdot-}$, superoxide anion radical; H_2O_2, hydrogen peroxide; DMSO, dimethyl sulfoxide; NADP$^+$, ß-nicotinamide adenine dinucleotide phosphate (oxidized form); CIP, calf intestine phosphatase; SOD, superoxide dismutase; CYP, cytochrome P450; G-6-PDH, glucose 6-phosphate dehydrogenase; G-6-P, glucose 6-phosphate; ROS, reactive oxygen species.

* Corresponding author. Tel.: +81 59 231 5011; fax: +81 59 231 5011.
E-mail address: kawanisi@doc.medic.mie-u.ac.jp (S. Kawanishi).

0006-2952/$ – see front matter © 2004 Elsevier Inc. All rights reserved.
doi:10.1016/j.bcp.2004.06.016

in mice [13,14]. Lipman et al. observed lymphomas in 77.9% of male C57BL/6 mice that received melatonin in the dose of 1.9 mg/mouse with food [13]. Leukemias were detected in 70–98% of C57BL/6 mice and in 78% of CC57Br mice treated subcutaneously with melatonin in the dose of 2.5 mg/mouse twice a week during 2.5–5 months. Noteworthily, it was appeared that melatonin being given in night drinking water relatively low dose (3–3.5 mg/kg) in mice was carcinogenic as well [14]. COMET assay showed that in pharmacological doses, melatonin induced DNA damage and cleavage in hamster ovarian cells [15]. Clastogenic effect of melatonin may be involved in the mechanism of its carcinogenic effect.

Judging from these results, melatonin may have the dual function of anticarcinogenic and carcinogenic potentials. Previously, we reported that antioxidants such as vitamin A and its derivative [16], vitamin E [17], quercetin [18], *N*-acetylcysteine [19] and curcumin [20] caused oxidative damage to cellular and isolated DNA. Virtually, some of putative chemopreventive antioxidants may have potential carcinogenicity. Then, we investigated the possibility that melatonin is metabolized to an ultimate carcinogen causing DNA damage. Melatonin is rapidly metabolized in the liver to its main metabolite, 6-hydroxymelatonin, by CYP1A2 [21,22]. In this study, we have examined whether 6-hydroxymelatonin causes DNA damage in the presence of Cu(II), using [^{32}P]-5′-end-labeled DNA fragments obtained from the human *p16* and *p53* tumor suppressor genes and the c-Ha-*ras*-1 protooncogene. These genes are suitable for studying the mechanisms of carcinogenesis because they are known to be targets for chemical carcinogens [23,24]. We also analyzed the formation of 8-oxo-7,8-dihydro-2′-deoxyguanosine (8-oxodG), a DNA lesion characteristic of oxidative damage, using an electrochemical detector coupled to a high-performance liquid chromatography (HPLC-ECD).

2. Materials and methods

2.1. Materials

The restriction enzymes (*Sma*I, *Bss*HII, *Eco*RI, *Apa*I and *Sty*I) and glucose 6-phosphate dehydrogenase (G-6-PDH) were purchased from Boehringer Mannheim GmbH (Germany). The restriction enzymes (*Hin*dIII and *Xba*I) and T_4 polynucleotide kinase were obtained from New England Biolabs (Beverly, MA). [γ-^{32}P]ATP (222 TBq/mmol) was acquired from New England Nuclear (Boston, MA). Diethylenetriamine-*N*,*N*,*N*′,*N*″,*N*″-pentaacetic acid (DTPA) and bathocuproine disulfonic acid were procured from Dojin Chemical Co. (Kumamoto, Japan). Acrylamide, piperidine, dimethyl sulfoxide (DMSO), bisacrylamide, β-nicotinamide adenine dinucleotide phosphate (oxidized form) ($NADP^+$) and glucose 6-phosphate monosodium salt (G-6-P) were purchased from Wako (Osaka, Japan). Cytochrome P450 (CYP) reductase (10.0 mg/mL protein from human microsomes) was purchased from Gentest Corporation (Woburn, MA). $CuCl_2$, ethanol, D-mannitol and sodium formate were acquired from Nacalai Tesque (Kyoto, Japan). Calf thymus DNA, calf intestine phosphatase (CIP), bacterial alkaline phosphatase (82 units/mg from *Escherichia coli*), superoxide dismutase (SOD, 3000 units/mg from bovine erythrocytes) and catalase (45,000 units/mg from bovine liver) were obtained from Sigma Chemical Co. (St. Louis, MO). 6-Hydroxymelatonin was obtained from Aldrich Chemical Co. (Milwaukee, IL). Nuclease P_1 (400 units/mg) was purchased from Yamasa Shoyu Co. (Chiba, Japan). *E. coli* formamidopyrimidine-DNA glycosylase (Fpg) was obtained from Trevigen Inc. (Gaithersburg, MD).

2.2. Preparation of ^{32}P-5′-end-labeled DNA fragments

Exon-containing DNA fragments were obtained from the human *p53* tumor suppressor gene [25]. The 5′-end-labeled 650-base-pair fragment (*Hin*dIII*13972–*Eco*RI*14621) was obtained by dephosphorylation with calf intestine phosphatase and rephosphorylation with [γ-^{32}P]ATP and T_4 polynucleotide kinase. The 650-base-pair fragment was further digested with *Apa*I to obtain a singly labeled 443-base-pair fragment (*Apa*I 14179–*Eco*RI*14621) and a 211-base-pair fragment (*Hin*dIII*13972–*Apa*I 14182) [26]. Exon-containing DNA fragments were also obtained from the human *p16* tumor suppressor gene [27]; these fragments were subcloned into the pGEM®-T Easy Vector (Promega Corporation) [28]. The 484-base-pair fragment (*Eco*RI*9466–*Eco*RI*9949) was further digested with *Bss*HII to obtain a singly labeled 324-base-pair fragment (*Eco*RI*9466–*Bss*HII 9789) and a 158-base-pair fragment (*Bss*HII 9794–*Eco*RI*9949). Furthermore, we prepared DNA fragments from the human c-Ha-*ras*-1 protooncogene [29], utilizing the plasmid, pbcNI. This plasmid carries a 6.6-kb *Bam*HI chromosomal DNA segment containing the c-Ha-*ras*-1 gene [30]. A singly labeled 341-base-pair fragment (*Xba*I 1906–*Ava*I* 2246), a 261-base-pair fragment (*Ava*I* 1645–*Xba*I 1905) and a 337-base-pair fragment (*Pst*I 2345–*Ava*I* 2681) were obtained as described previously [29]. Nucleotide numbering for the human c-Ha-*ras*-1 protooncogene begins with the *Bam*HI site [30]. Asterisks indicate ^{32}P-labeling.

2.3. Detection of DNA damage by 6-hydroxymelatonin in the presence of metal ion

Standard reaction mixtures (in a 1.5 mL Eppendorf microtube) containing [^{32}P]-5′-end-labeled DNA fragments, calf thymus DNA (20 μM/base), 20 μM $CuCl_2$ and 6-hydroxymelatonin in 200 μL of 10 mM sodium phosphate buffer (pH 7.8) containing 5 μM DTPA were incubated for 2 h at 37 °C. Subsequently, the DNA was

treated with 1 M piperidine for 20 min at 90 °C or 10 units of Fpg protein in the reaction buffer (10 mM HEPES-KOH (pH 7.4), 100 mM KCl, 10 mM EDTA and 0.1 mg/mL BSA) for 2 h at 37 °C. Fpg protein catalyzes the excision of 8-oxodG as well as Fapy residues [31–33]. After ethanol precipitation, the DNA fragments were electrophoresed and the autoradiogram was obtained by exposing X-ray film to the gel as described previously [29]. The preferred cleavage sites were determined by direct comparison of the positions of the oligonucleotides with those produced by the chemical reactions of the Maxam–Gilbert procedure [34] using a DNA-sequencing system (LKB 2010 Macrophor). A laser densitometer (LKB 2222 UltroScan XL) was used for the measurement of the relative amounts of oligonucleotides from the treated DNA fragments.

2.4. Analysis of 8-oxodG formation in calf thymus DNA by 6-hydroxymelatonin

The quantity of 8-oxodG was measured utilizing a modification of the method described by Kasai et al. [35]. Standard reaction mixtures (in a 1.5 mL Eppendorf microtube) containing indicated concentrations of 6-hydroxymalatonin and calf thymus DNA fragments (100 μM/base) in 400 μL of 4 mM sodium phosphate buffer (pH 7.8) containing 5 μM DTPA were incubated for 2 h at 37 °C. Following ethanol precipitation, the DNA fragments were digested into the nucleosides with nuclease P_1 and calf intestine phosphate, and then analyzed by HPLC-ECD, as described previously [36]. Data represent the means ± S.D. of four independent experiments.

2.5. Measurement of oxygen consumption

Oxygen consumption by the reactions of 6-hydroxymelatonin with Cu(II) was measured using a Clarke oxygen electrode (Electronic Stirrer Model 300, Rank Brothers LTD. Bottisham Cambridge, England). The mixture contained 6-hydroxymelatonin and 4% (v/v) of ethanol in 2 mL of 10 mM sodium phosphate buffer (pH 7.8), containing 2.5 μM DTPA. Where indicated,CYP reductase was added to examine the formation of the redox cycle resulting from oxygen consumption. The reactions were started by the addition of 20 μM $CuCl_2$ into the chamber of the oxygen electrode.

2.6. Analysis of 8-oxodG formation in human cultured cells

HL-60 and HP100 cells were grown in RPMI 1640 supplemented with 6% FBS at 37 °C under 5% CO_2 in a humidified atmosphere. Catalase activity of HP100 cells was 18 times higher than that of HL-60 cells [37]. HL-60 and HP100 cells (10^6 cells/mL) were incubated with various concentrations of 6-hydroxymelatonin for 4 h. Where indicated, HL-60 cells (10^6 cells/mL) were preincubated with 0.2 mM *o*-phenanthroline or bathocuproine for 30 min, followed by incubation with 5 μM 6-hydroxymelatonin for 4 h at 37 °C. After the incubation, the medium was removed, and the cells were washed three times with cold phosphate-buffered saline (PBS). We isolated DNA from cells and digested DNA into nucleosides under complete anaerobic conditions using anaerobic incubator, which carried out the trap of the oxygen of very small quantity. The cells were suspended in 0.05 mg/mL RNase, 0.5 mg/mL proteinase K, and 500 μL of lysis buffer (Applied Biosystems), followed by incubation for 1 h at 60 °C. After ethanol precipitation, DNA was digested to the nucleosides with 8 units of nuclease P_1 and 1.2 units of bacterial alkaline phosphatase in anaerobiosis. The resulting 2′-deoxyribonucleosides mixture was injected into an HPLC apparatus (SCL-10AV, Shimadzu, Kyoto, Japan) equipped with both a UV detector (SPD-10AV, Shimadzu) and an electrochemical detector (Coulochem II, ESA, MA, USA): column, CAPCELL PAK C18 MG (0.46 × 15 cm) (Shiseido, Tokyo, Japan); eluent, 8% aqueous methanol containing 10 mM NaH_2PO_4; flow rate 1 mL/min. The molar ratio of 8-oxodG to 2′-deoxyguanosine (dG) in each DNA sample was measured based on the peak height of authentic 8-oxodG with the electrochemical detector and the UV absorbance at 254 nm of dG [36].

3. Results

3.1. Damage to ^{32}P-labeled DNA fragments by 6-hydroxymelatonin in the presence of metal ion

In the presence of Cu(II), 6-hydroxymelatonin induced DNA damage in a dose-dependent manner (Fig. 1A). 6-Hydroxymelatonin alone or melatonin could not cause DNA damage (data not shown). When cytochrome P450 (CYP) reductase was added, DNA damage was enhanced (Fig. 1A). Even without piperidine treatment, oligonucleotides were formed by 6-hydroxymelatonin in the presence of Cu(II), indicating breakage of the deoxyribose phosphate backbone (Fig. 1B, lanes 2–4). Piperidine treatment increased the formation of smaller size oligonucleotides (Fig. 1B, lanes 8–10). Since altered base is readily removed from its sugar by the piperidine treatment, it is considered that the base modification was induced by 6-hydroxymelatonin in the presence of Cu(II). Furthermore, the formation of Fpg-sensitive sites by 6-hydroxymelatonin in the presence of Cu(II) significantly increased compared with the yield of strand breaks (Fig. 1B, lanes 2–7). On the other hand, the Fpg-sensitive site formation by H_2O_2 and Fe(II) was not significantly increased compared with the yield of strand breaks (Fig. 1B, lanes 11–14). 6-Hydroxymelatonin did not induce DNA damage in the presence of other metal ions, including Co(II), Ni(II), Mn(II), Mn(III), Fe(III) and Fe(III)EDTA (data not shown).

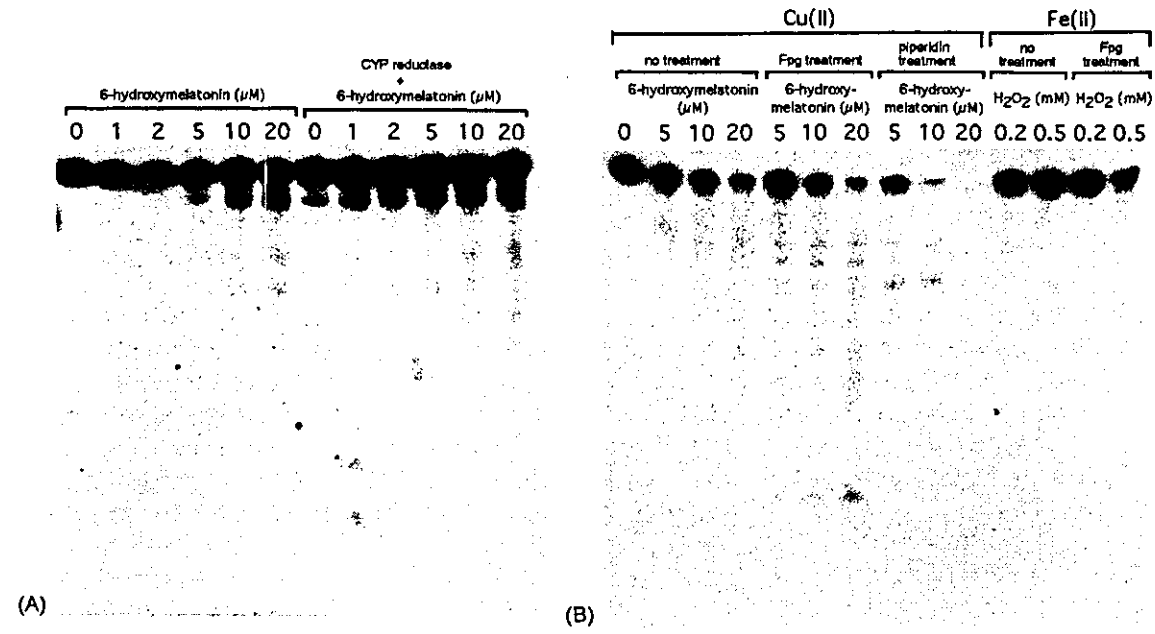

Fig. 1. Autoradiogram of ^{32}P-labeled DNA fragments incubated with 6-hydroxymelatonin plus Cu(II). (A) The reaction mixtures (in a 1.5 mL Eppendorf microtube) containing indicated concentrations of 6-hydroxymelatonin, ^{32}P-5′-end-labeled 158-base-pair DNA fragments, 20 μM/base of calf thymus DNA, 20 μM $CuCl_2$, 0.25 nM CYP450 reductase, 250 μM $NADP^+$, 500 μM G-6-P, 0.07 units G-6-PDH and 500 μM $MgCl_2$ in 200 μL of 10 mM sodium phosphate buffer (pH 7.8) containing 5 μM DTPA were incubated for 2 h at 37 °C. Subsequently, DNA fragments were treated with 1 M piperidine for 20 min at 90 °C, then electrophoresed on an 8% polyacrylamide/8 M urea gel. (B) The reaction mixtures (in a 1.5 mL Eppendorf microtube) containing ^{32}P-5′-end-labeled 261-base-pair DNA fragments, 20 μM/base of calf thymus DNA, 6-hydroxymelatonin plus 20 μM $CuCl_2$ or H_2O_2 plus 20 μM $FeSO_4(NH_4)_2SO_4$ in 200 μL of 10 mM sodium phosphate buffer (pH 7.8) containing 5 μM DTPA were incubated for 2 h at 37 °C. Subsequently, DNA fragments were treated with or without Fpg protein or with 1 M piperidine, and then electrophoresed on an 8% polyacrylamide/8 M urea gel. The autoradiogram was visualized by exposing an X-ray film to the gel.

3.2. Effects of scavengers and a metal chelator on DNA damage induced by 6-hydroxymelatonin

To examine the molecular mechanism of DNA damage, we evaluated the effects of scavengers and a metal chelator on DNA damage induced by 6-hydroxymelatonin in the presence of Cu(II) (Fig. 2). Catalase and bathocuproine, a Cu(I)-specific chelator, inhibited DNA damage by 6-hydroxymelatonin, suggesting the involvement of H_2O_2 and Cu(I). Free hydroxyl radical (•OH) scavengers, such as ethanol, mannitol, sodium formate and DMSO, demonstrated little or no inhibitory effect on DNA damage by 6-hydroxymelatonin. Methional inhibited DNA damage. Methional is capable of scavenging both •OH and species with weaker reactivity [38,39].

3.3. Site specificity of DNA cleavage by 6-hydroxymelatonin

DNA cleavage sites were identified by a direct comparison of the oligonucleotide positions produced by 6-hydroxymelatonin with those produced by the Maxam–Gilbert procedure [34]. ^{32}P-5′-end-labeled DNA fragments were treated with 6-hydroxymelatonin in the presence of Cu(II). An autoradiogram was obtained and scanned with a laser densitometer to measure relative intensity of DNA cleavage in the c-Ha-*ras*-1 protooncogene (Fig. 3A) and the human *p53* tumor suppressor gene (Fig. 3B). 6-Hydroxymelatonin induced piperidine-labile sites preferentially at thymine and cytosine residues (Fig. 3). With Fpg treatment, the DNA cleavage occurred mainly at guanine and cytosine residues. 6-Hydroxymelatonin caused piperidine-labile and Fpg sensitive lesions at C and G in the 5′-ACG-3′ sequence, a well-known hotspot of the *p53* gene [23,40] (Fig. 3B). From these results, it is considered that 6-hydroxymelatonin can cause DNA damage at 5′-TG-3′ and 5′-CG-3′ sequences at high frequency.

3.4. Formation of 8-oxodG in calf thymus DNA by 6-hydroxymelatonin in the presence of Cu(II)

Using an HPLC-ECD, we measured the quantity of 8-oxodG, an indicator of oxidative base damage [35,36], in calf thymus DNA following treatment with variable concentrations of 6-hydroxymelatonin in the presence of Cu(II). The level of 8-oxodG significantly increased with increasing concentrations of 6-hydroxymelatonin (Fig. 4). The addition of CYP reductase enhanced 6-hydroxymelatonin plus Cu(II)-induced 8-oxodG formation.

3.5. Oxygen consumption during Cu(II)-mediated autoxidation of 6-hydroxymelatonin and enhancement by CYP reductase

Fig. 5 shows oxygen consumption during the autoxidation of 6-hydroxymelatonin in the presence of Cu(II).

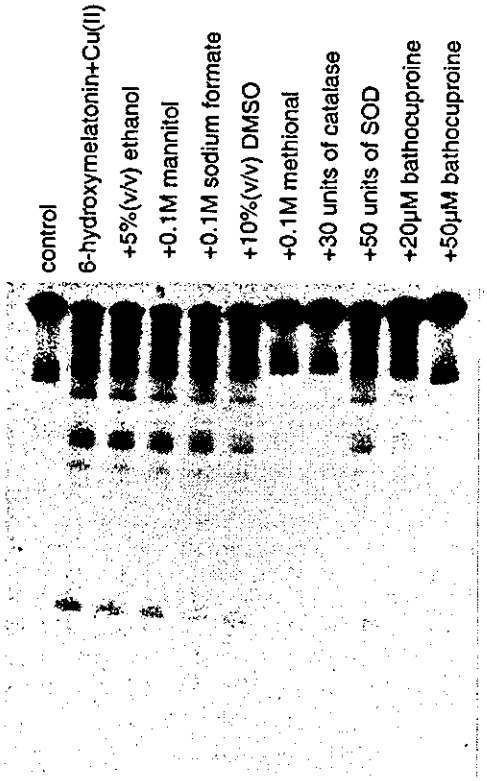

Fig. 2. Effects of scavengers and bathocuproine on the DNA damage induced by 6-hydroxymelatonin in the presence of Cu(II). Reaction mixtures contained the ^{32}P-5′-end-labeled 443-base-pair DNA fragment, 20 μM/base of calf thymus DNA, 20 μM 6-hydroxymelatonin and 20 μM $CuCl_2$ in 200 μL of 10 mM sodium phosphate buffer (pH 7.8) containing 5 μM DTPA. Reaction mixtures were incubated for 2 h at 37 °C. DNA fragments were treated with 1 M piperidine for 20 min at 90 °C, then electrophoresed on an 8% polyacrylamide/8 M urea gel. The autoradiogram was visualized by exposing an X-ray film to the gel.

When Cu(II) was added, 6-hydroxymelatonin consumed oxygen. The addition of CYP reductase increased oxygen consumption, suggesting that redox cycle was formed.

3.6. Formation of 8-oxodG in human cultured cells treated with 6-hydroxymelatonin

To investigate oxidative damage in cellular DNA, we measured the content of 8-oxodG in HL-60 and HP 100 cells treated with 6-hydroxymelatonin. Production of 8-oxodG in HL-60 cells was increased in a dose-dependent manner (Fig. 6A). The content of 8-oxodG in HL-60 cells treated with 2 μM 6-hydroxymelatonin was significantly larger in comparison with the control. However, 6-hydroxymelatonin did not increase the amount of 8-oxodG in HP100 cells (Fig. 6A). It was reported that HP100 cells were approximately 340-fold more resistant to H_2O_2 than the parent cell line, HL-60 [37]. These results suggest that generation of H_2O_2 plays a critical role in DNA damage.

To examine the possible role of endogenous cellular metal, bathocuproine or *o*-phenanthroline was added to HL-60 cells incubated with 6-hydroxymelatonin. The amounts of 8-oxodG induced by 5 μM 6-hydroxymelatonin were significantly reduced by the addition of bathocuproine or *o*-phenanthroline, confirming the involvement of metal, especially copper ion. (Fig. 6B).

4. Discussion

In this study, 6-hydroxymelatonin caused oxidative DNA damage in the presence of Cu(II). Experiments with piperidine or Fpg treatment revealed that C and G of the 5′-ACG-3′ sequence, the complementary sequence to codon 273 (a known hotspot) in exon 8 of the *p53* gene [23,40], were significantly damaged, although C was damaged to a lesser extent than the G. 6-Hydroxymelatonin also formed piperidine-labile lesions at T of the 5′-TG-3′ sequence. When DNA fragments were treated with Fpg protein, 6-hydroxymelatonin caused DNA damage mainly at G residues especially of the 5′-TG-3′ sequence. Fpg protein mainly catalyzes the excision of piperidine-resistant 8-oxodG [31] and further oxidized piperidine-labile guanine residues [41], although Fpg also mediates cleavage of uracil glycol [42], 5-hydroxycytosine and 5,6-dihydrothymine [43], in vitro. Therefore, it is reasonably considered that 6-hydroxymelatonin oxidizes the G residue of 5′-CG-3′ and 5′-TG-3′ sequences to 8-oxodG. Although, it is postulated that double-base lesions can be generated from one radical hit [44–46], further work is required to ascertain whether the putative double-base lesion with DNA is present or not.

We demonstrated that the content of 8-oxodG in HL-60 cells was increased by the 6-hydroxymelatonin treatment, whereas the content of 8-oxodG in HP100 cells was not increased. The catalase activity of HP100 cells was 18 times higher than that of HL-60 cells [37]. Therefore, it is considered that generation of H_2O_2 plays an important role in 6-hydroxymelatonin-induced 8-oxodG formation in human cultured cells. Furthermore, the formation of 8-oxodG was markedly reduced by *o*-phenanthroline or bathocuproine, suggesting that copper ion may be involved in oxidative DNA damage by 6-hydroxymelatonin in the cells.

To clarify what kinds of reactive species were involved in DNA damage by 6-hydroxymelatonin, we examined the effects of scavengers on DNA damage. The inhibitory effects of catalase and bathocuproine on 6-hydroxymelatonin-induced DNA damage suggest that both H_2O_2 and Cu(I) participate in DNA damage. Typical $^{\bullet}$OH scavengers demonstrated little or no inhibitory effect, whereas methional inhibited DNA damage. This result suggests the involvement of reactive species with a similar reactivity to $^{\bullet}$OH [38,39]. Piperidine-labile DNA lesion by 6-hydroxymelatonin with Cu(II) occurred predominantly at thymine and cytosine residues. Furthermore, the yield of Fpg-sensitive sites, such as 8-oxodG, by 6-hydroxymelatonin significantly increased compared with the yield of strand breaks. $^{\bullet}$OH induces DNA cleavage without a nucleotide bias

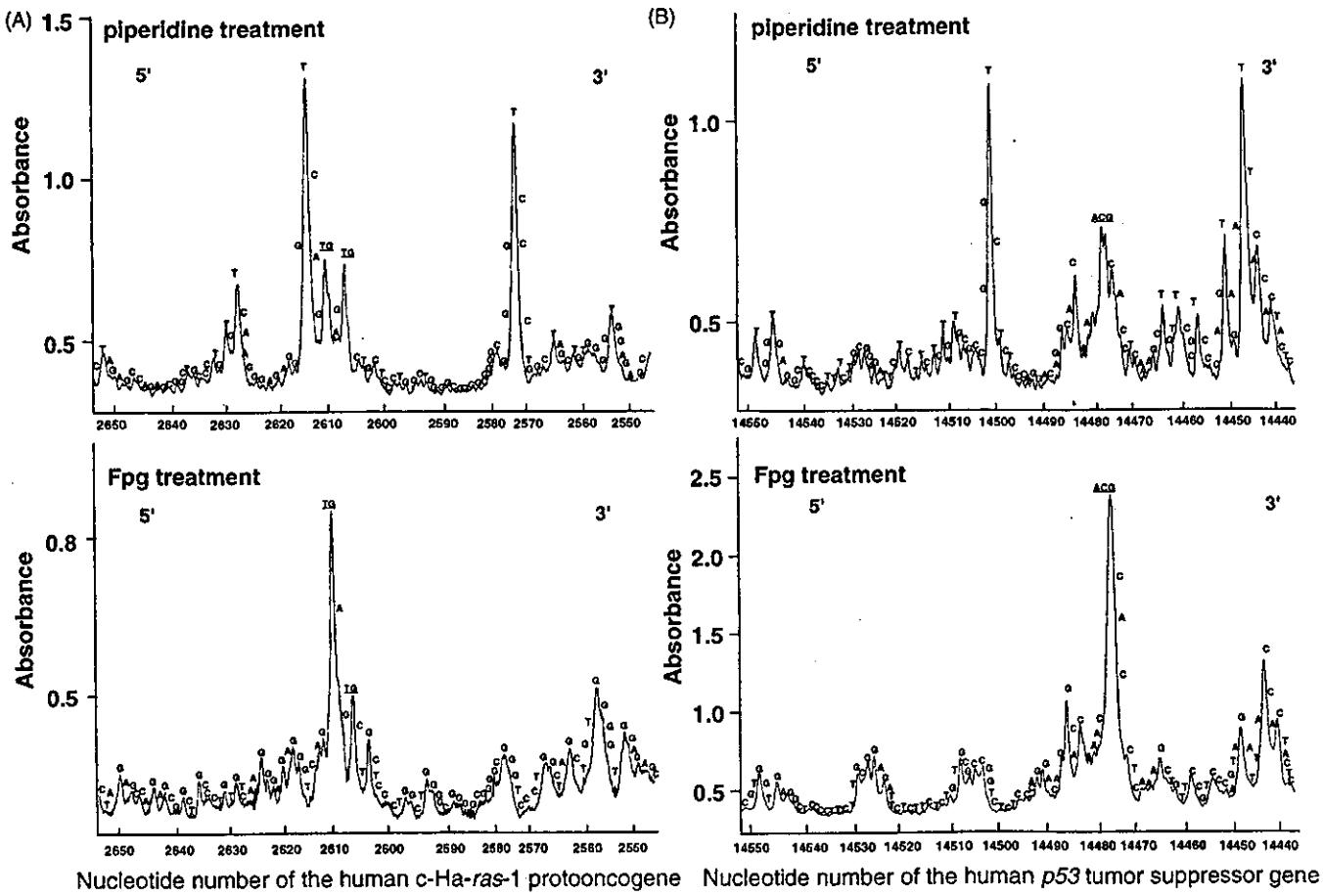

Fig. 3. Site specificity of DNA cleavage induced by 6-hydroxymelatonin in the presence of Cu(II). Reaction mixtures contained either the ^{32}P-5′-end-labeled 443-base-pair fragment (*Apa*I 14179–*Eco*RI*14621) derived from the human *p53* tumor suppressor gene (A) or the 337-base-pair fragment (*Pst*I 2345–*Ava*I* 2681) derived from the human c-Ha-*ras*-1 protooncogene (B), 20 μM/base of calf thymus DNA, 20 μM 6-hydroxymelatonin and 20 μM $CuCl_2$ in 200 μL of 10 mM sodium phosphate buffer (pH 7.8) containing 5 μM DTPA. Reaction mixtures were incubated for 2 h at 37 °C. Following piperidine or Fpg treatment, the DNA fragments were analyzed as described in Fig. 1 legend. The relative quantities of oligonucleotides were measured by scanning the autoradiogram with a laser densitometer (LKB 2222 UltroScan XL, Pharmacia Biotech). Underlined bases represent double-base lesions detected by the treatment with piperidine and Fpg protein.

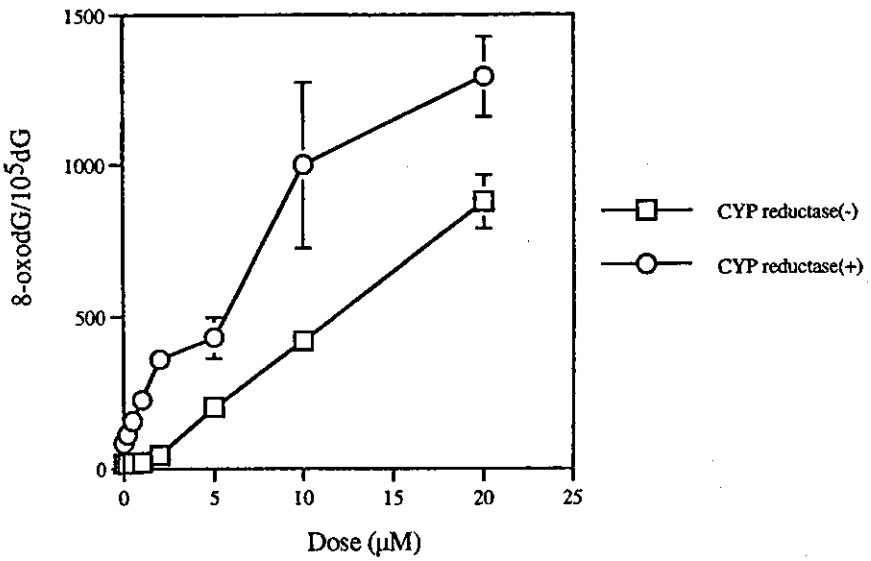

Fig. 4. Formation of 8-oxodG by 6-hydroxymelatonin in the presence of Cu(II). Standard reaction mixtures (in a 1.5 mL Eppendorf microtube) containing indicated concentrations of 6-hydroxymelatonin, 0.25 nM CYP450 reductase, 250 μM $NADP^+$, 500 μM G-6-P, 0.07 units G-6-PDH and 500 μM $MgCl_2$ in 400 μL of 4 mM sodium phosphate buffer (pH 7.8) containing 5 μM DTPA were incubated for 2 h at 37 °C. Following an incubation, 0.2 mM DTPA was added to stop the reaction and then the DNA was precipitated in ethanol. The DNA was subjected to enzymatic digestion and analyzed by HPLC-ECD.

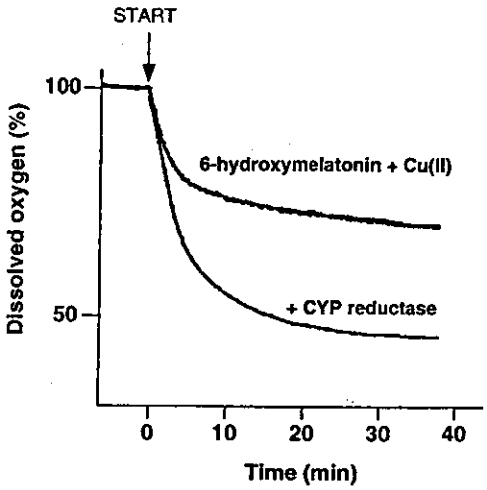

Fig. 5. Oxygen consumption by the interaction of 6-hydroxymelatonin with Cu(II). The mixture contained 6-hydroxymelatonin and 4% (v/v) of ethanol in 2 mL of 10 mM sodium phosphate buffer (pH 7.8), containing 2.5 μM DTPA at 37 °C. Where indicated, to detect redox cycle formation, 0.57 nM CYP reductase, 250 μM $NADP^+$, 500 μM G-6-P, 0.07 units G-6-PDH and 500 μM $MgCl_2$ were added. The reactions were started by the addition of 20 μM $CuCl_2$ into the chamber of the oxygen electrode (indicated by an arrow).

[47,48]. Thus, $^{\bullet}OH$ does not appear to play an important role in DNA damage by 6-hydroxymelatonin. This is supported by papers showing that the levels of 8-oxodG relative to strand breaks produced by Cu(II)/H_2O_2 were higher than that produced by Fe(II)-EDTA/H_2O_2 and γ-radiation [49,50]. Therefore, it is considered that reactive species formed from H_2O_2 and Cu(I) are involved in DNA damage by 6-hydroxymelatonin.

On the basis of this study, we propose a possible mechanism whereby melatonin induces Cu(II)-mediated DNA damage (Fig. 7). CYPs are contained in the lung, lymph nodes, liver and skin [51]. Melatonin undergoes CYP 1A2-catalyzed 6-hydroxylation to 6-hydroxymelatonin [21,22]. 6-Hydroxymelatonin undergoes Cu(II)-catalyzed autoxidation into the corresponding radical, leading to the production of the quinone methide form. Relevantly, Hadi et al. have reported that a high concentration of 5-hydroxytryptamine (serotonin), which is structurally related to 6-hydroxymelatonin, can reduce two molar equivalents of Cu(II) to Cu(I) through a reaction involving two electron oxidation of the phenol to a quinone methide [52]. During the autoxidation of 6-hydroxymelatonin, Cu(II) is reduced to Cu(I), which reacts with O_2 to generate O_2^- and subsequently H_2O_2. H_2O_2 interacts with Cu(I) to form the Cu(I)-hydroperoxo complex, capable of inducing DNA damage [53]. CYP reductase enhanced O_2 consumption, suggesting that redox cycle was formed and O_2^- generation was enhanced, leading to enhancement of oxidative DNA damage. Some quinones can undergo enzymatic and non-enzymatic redox cycling with their corresponding semiquinone radicals and generate O_2^- [54–56]. Previously, we have also reported that catechol-type compounds (quercetin, catechol, curcumin) efficiently generated reactive oxygen species (ROS) in the presence of metal ion via redox cycle [19,21,57,58]. We have demonstrated that NAD(P)H may non-enzymatically reduce *o*-quinones to catechols through two-electron reduction [57,58]. In this paper, newly we showed the non-catechol type compound (6-hydroxymelatonin) is also

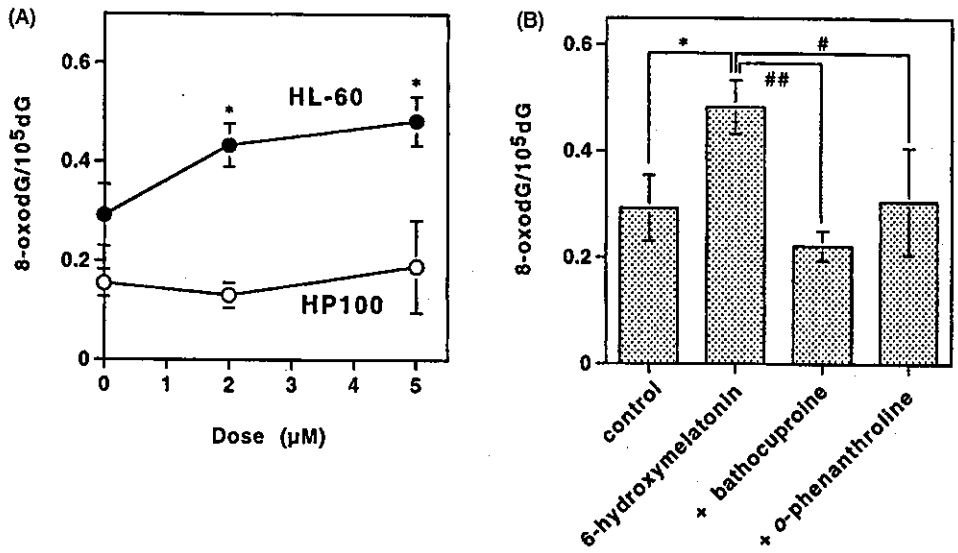

Fig. 6. Formation of 8-oxodG by 6-hydroxymelatonin in human cultured cells and the inhibitory effects of bathocuproine and *o*-phenanthroline. HL-60 (closed symbol) and HP100 (open symbol) cells (10^6 cells/mL) were incubated with various concentrations of 6-hydroxymelatonin for 4 h (A). HL-60 cells (10^6 cells/mL) were preincubated with 0.2 mM *o*-phenanthroline or bathocuproine for 30 min, followed by incubation with 5 μM 6-hydroxymelatonin for 4 h at 37 °C (B). After the incubation, DNA was extracted immediately. And then, the DNA was subjected to enzyme digestion and analyzed by HPLC-ECD as described in Materials and methods. Results are expressed as means ± S.D. of values obtained from four independent experiments. The asterisk indicates significant differences compared with the control by *t*-test ($^{*}P < 0.01$). $^{\#}P < 0.05$ and $^{\#\#}P < 0.001$, significantly decreased by the addition of *o*-phenanthroline or bathocuproine.

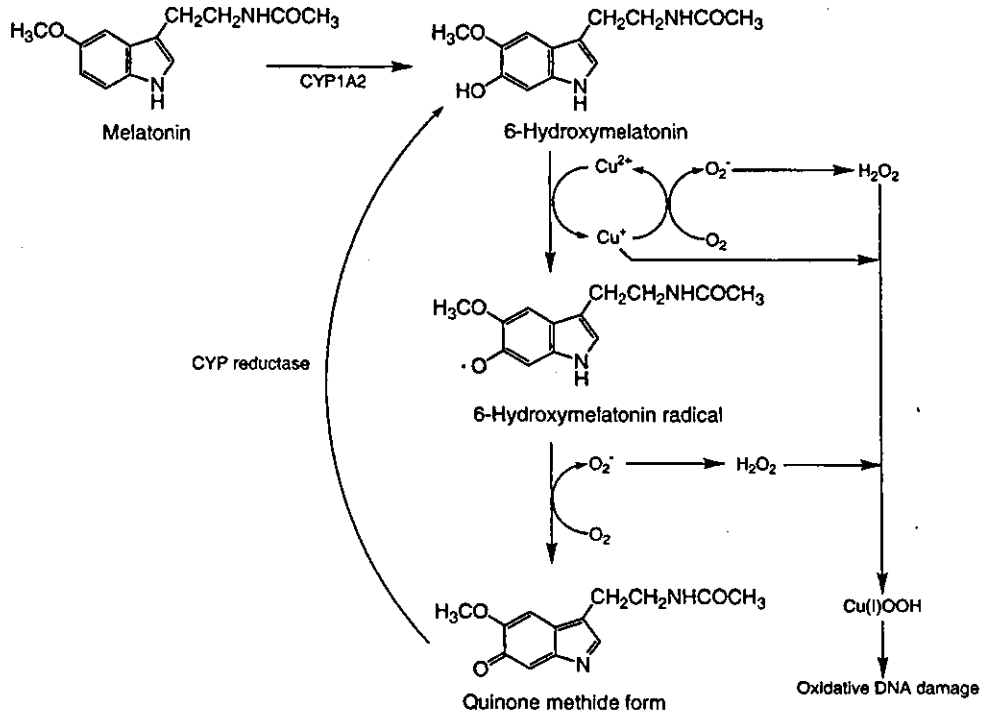

Fig. 7. A possible mechanism for Cu(II)-mediated DNA damage induced by melatonin.

autooxidated by the copper ion and found that 6-hydroxymelatonin enzymatically induced oxidative DNA damage via non-quinone type of redox cycle.

Copper exists in the mammalian cell nucleus, and may contribute to high-order chromatin structures [59]. Copper ions bind to non-histone proteins, and cause much stronger ascorbate-mediated DNA damage than iron [60]. Copper has the ability to catalyze the production of reactive oxygen species to mediate oxidative DNA damage [61–63]. Therefore, it is reasonably concluded that Cu(II) ion may participate in reactive oxygen generation under certain conditions, although mammals have evolved means of minimizing levels of free copper ions and most copper ions bind to protein carriers and transporters [64]. These studies support the finding that a melatonin metabolite caused DNA damage by generating ROS through the interaction with copper. On the other hand, several papers suggested that DNA damage was caused by H_2O_2 through an in vivo Fenton reaction [65,66]. Consequently, there still remains another possibility that Fe(II) participates in melatonin-induced DNA damage in the cells.

Melatonin and 6-hydroxymelatonin are known to be effective as free radical scavengers and have an anti-cancer effect [3–11]. On the other hand, it has been reported that long-term night administration of melatonin significantly increases malignant tumor incidence in female CBA mice [14]. In this study, we have demonstrated that a melatonin metabolite, 6-hydroxymelatonin, can cause oxidative DNA damage, probably double-base lesions at 5′-CG-3′ and 5′-TG-3′ sequences. We have also shown that G residue in 5′-CG-3′ and 5′-TG-3′ sequences was oxidized to 8-oxodG, which can cause the misreplication of DNA (G:C→T:A transversion) that might lead to mutation or cancer [67–69]. Findings of DNA damage by 6-hydroxymelatonin itself via a new type of redox cycle may provide an insight into mechanism of carcinogenesis by melatonin through ROS formation, in addition to already known types of DNA damage. Further study on safety should be required when melatonin is used for cancer prevention or nutrition supplement in humans.

Acknowledgement

This work was supported by Japan Health Foundation, Health Research Foundation and Grants-in-Aid for Scientific Research from the Ministry of Education, Science, Sports and Culture of Japan.

References

[1] Arendt J, Symons AM, Laud CA, Pryde SJ. Melatonin can induce early onset of the breeding season in ewes. J Endocrinol 1983;97:395–400.

[2] Reiter RJ. Pineal melatonin: cell biology of its synthesis and of its physiological interactions. Endocr Rev 1991;12:151–80.

[3] Reiter RJ, Melchiorri D, Sewerynek E, Poeggeler B, Barlow-Walden L, Chuang J, et al. A review of the evidence supporting melatonin's role as an antioxidant. J Pineal Res 1995;18:1–11.

[4] Barlow-Walden LR, Reiter RJ, Abe M, Pablos M, Menendez-Pelaez A, Chen LD, et al. Melatonin stimulates brain glutathione peroxidase activity. Neurochem Int 1995;26:497–502.

[5] Noda Y, Mori A, Liburdy R, Packer L. Melatonin and its precursors scavenge nitric oxide. J Pineal Res 1999;27:159–63.
[6] Mocchegiani E, Bulian D, Santarelli L, Tibaldi A, Muzzioli M, Pierpaoli W, et al. The immuno-reconstituting effect of melatonin or pineal grafting and its relation to zinc pool in aging mice. J Neuroimmunol 1994;53:189–201.
[7] Pierpaoli W, Regelson W. Pineal control of aging: effect of melatonin and pineal grafting on aging mice. Proc Natl Acad Sci USA 1994;91:787–91.
[8] Bartsch H, Buchberger A, Franz H, Bartsch C, Maidonis I, Mecke D, et al. Effect of melatonin and pineal extracts on human ovarian and mammary tumor cells in a chemosensitivity assay. Life Sci 2000;67:2953–60.
[9] Matsubara E, Shoji M, Murakami T, Kawarabayashi T, Abe K. Alzheimer's disease and melatonin. Int Congr Ser 2003;1252: 395–8.
[10] Beyer CE, Steketee JD, Saphier D. Antioxidant properties of melatonin-an emerging mystery. Biochem Pharmacol 1998;56:1265–72.
[11] Reiter R, Tang L, Garcia JJ, Munoz-Hoyos A. Pharmacological actions of melatonin in oxygen radical pathophysiology. Life Sci 1997;60:2255–71.
[12] Tailleux A, Torpier G, Bonnefont-Rousselot D, Lestavel S, Lemdani M, Caudeville B, et al. Daily melatonin supplementation in mice increases atherosclerosis in proximal aorta. Biochem Biophys Res Commun 2002;293:1114–23.
[13] Lipman RD, Bronson RT, Wu D, Smith DE, Prior R, Cao G, et al. Disease incidence and longevity are unaltered by dietary antioxidant supplementation initiated during middle age in C57BL/6 mice. Mech Ageing 1998;103:269–84.
[14] Anisimov VN, Zavarzina NI, Zabezhinskii MA, Popovich IG, Anikin IV, Zimina OA, et al. The effect of melatonin on the indices of biological age, on longevity and on the development of spontaneous tumors in mice. Vopr Onkol 2000;46:311–9.
[15] Musatov SA, Anisimov VN, Andre V, Vigreux C, Godard T, Gauduchon P, et al. Modulatory effects of melatonin on genotoxic response of reference mutagens in the Ames test and the comet assay. Mutat Res 1998;417:75–84.
[16] Murata M, Kawanishi S. Oxidative DNA damage by vitamin A and its derivative via superoxide generation. J Biol Chem 2000;275:2003–8.
[17] Yamashita N, Murata M, Inoue S, Burkitt MJ, Milne L, Kawanishi S. α-tocopherol induces oxidative damage to DNA in the presence of copper(II) ions. Chem Res Toxicol 1998;11:855–62.
[18] Yamashita N, Kawanishi S. Distinct mechanisms of DNA damage in apoptosis induced by quercetin and luteolin. Free Radical Res 2000;33:623–33.
[19] Oikawa S, Yamada K, Yamashita N, Tada-Oikawa S, Kawanishi S. *N*-acetylcysteine, a cancer chemopreventive agent, causes oxidative damage to cellular and isolated DNA. Carcinogenesis 1999;20: 1485–90.
[20] Sakano K, Kawanishi S. Metal-mediated DNA damage induced by curcumin in the presence of human cytochrome P450 isozymes. Arch Biochem Biophys 2002;405:223–30.
[21] Skene DJ, Papagiannidou E, Hashemi E, Snelling J, Lewis DF, Fernandez M, et al. Contribution of CYP1A2 in the hepatic metabolism of melatonin: studies with isolated microsomal preparations and liver slices. J Pineal Res 2001;31:333–42.
[22] Matuszak Z, Reszka K, Chignell CF. Reaction of melatonin and related indoles with hydroxyl radicals: EPR and spin trapping investigations. Free Radic Biol Med 1997;23:367–72.
[23] Denissenko MF, Pao A, Tang M, Pfeifer GP. Preferential formation of benzo[a]pyrene adducts at lung cancer mutational hotspots in *p53*. Science 1996;274:430–2.
[24] Wei SJ, Chang RL, Merkler KA, Gwynne M, Cui XX, Murthy B, et al. Dose-dependent mutation profile in the c-Ha-ras proto-oncogene of skin tumors in mice initiated with benzo[a]pyrene. Carcinogenesis 1999;20:1689–96.
[25] Chumakov P. EMBL Data Library, accession number X54156; 1990.
[26] Yamashita N, Murata M, Inoue S, Hiraku Y, Yoshinaga T, Kawanishi S. Superoxide formation and DNA damage induced by a fragrant furanone in the presence of copper(II). Mutat Res 1998;397:191–201.
[27] Serrano M, Hannon GJ, Beach DA. A new regulatory motif in cell-cycle control causing specific inhibition of cyclin D/CDK4. Nature 1993;366:704–7.
[28] Oikawa S, Murakami K, Kawanishi S. Oxidative damage to cellular and isolated DNA by homocysteine: implications for carcinogenesis. Oncogene 2003;22:3530–8.
[29] Yamamoto K, Kawanishi S. Hydroxyl free radical is not the main active species in site-specific DNA damage induced by copper (II) ion and hydrogen peroxide. J Biol Chem 1989;264:15435–40.
[30] Capon DJ, Chen EY, Levinson AD, Seeburg PH, Goeddel DV. Complete nucleotide sequences of the T24 human bladder carcinoma oncogene and its normal homologue. Nature 1983;302:33–7.
[31] David-Cordonnier MH, Laval J, O'Neill P. Clustered DNA damage, influence on damage excision by XRS5 nuclear extracts and *Escherichia coli* Nth and Fpg proteins. J Biol Chem 2000;275:11865–73.
[32] Boiteux S, Gajewskim E, Laval J, Dizdaroglu M. Substrate specificity of the *Escherichia coli* Fpg protein (formamidopyrimidine-DNA glycosylase): excision of purine lesions in DNA produced by ionizing radiation or photosensitization. Biochemistry 1992;31:106–10.
[33] Bruner SD, Norman DP, Verdine GL. Structural basis for recognition and repair of the endogenous mutagen 8-oxoguanine in DNA. Nature 2000;403:859–66.
[34] Maxam AM, Gilbert W. Sequencing end-labeled DNA with base-specific chemical cleavages. Methods Enzymol 1980;65:499–560.
[35] Kasai H, Crain PF, Kuchino Y, Nishimura S, Ootsuyama A, Tanooka H. Formation of 8-hydroxyguanine moiety in cellular DNA by agents producing oxygen radicals and evidence for its repair. Carcinogenesis 1986;7:1849–51.
[36] Ito K, Inoue S, Yamamoto K, Kawanishi S. 8-Hydroxydeoxyguanosine formation at the 5' site of 5'-GG-3' sequences in double-stranded DNA by UV radiation with riboflavin. J Biol Chem 1993;268:13221–7.
[37] Kasugai I, Yamada M. High production of catalase in hydrogen peroxide-resistant human leukemia HL-60 cell lines. Leukemia Res 1992;16:173–9.
[38] Schweigert N, Acero JL, von Gunten U, Canonica S, Zehnder AJ, Eggen RI. DNA degradation by the mixture of copper and catechol is caused by DNA-copper-hydroperoxo complexes, probably DNA-Cu(I)OOH. Environ Mol Mutagen 2000;36:5–12.
[39] Kawanishi S, Hiraku Y, Murata M, Oikawa S. The role of metals in site-specific DNA damage with reference to carcinogenesis. Free Radic Biol Med 2002;32:822–32.
[40] Hollstein M, Sidransky D, Vogelstein B, Harris CC. *p53* mutations in human cancers. Science 1991;253:49–53.
[41] Gasparutto D, Ravanat JL, Gérot O, Cadet J. Characterization and chemical stability of photooxidized oligonucleotides that contain 2,2-diamino-4-[(2-deoxy-ß-D-erythro-pentofuranosy)amino]-5(2H)-oxazolone. J Am Chem Soc 1998;120:10283–6.
[42] Purmal AA, Lampman GW, Bond JP, Hatahet Z, Wallace SS. Enzymatic processing of uracil glycol, a major oxidative product of DNA cytosine. J Biol Chem 1998;273:10026–35.
[43] D'Ham C, Romieu A, Jaquinod M, Gasparutto D, Cadet J. Excision of 5,6-dihydroxy-5,6-dihydrothymine, 5,6-dihydrothymine, and 5-hydroxycytosine from defined sequence oligonucleotides by *Escherichia coli* endonuclease III and Fpg proteins: kinetic and mechanistic aspects. Biochemistry 1999;38:3335–44.
[44] Box HC, Dawidzik JB, Budzinski EE. Free radical-induced double-base lesions in DNA. Free Radic Biol Med 2001;31:856–68.
[45] Bourdat AG, Douki T, Frelon S, Gasparutto D, Cadet J. Tandem base lesions are generated by hydroxyl radical within isolated DNA in aerated aqueous solution. J Am Chem Soc 2000;122:4549–56.
[46] Douki T, Riviere J, Cadet J. DNA tandem lesions containing 8-oxo-7, 8-dihydroguanine and formamido residues arise from intramolecular